AD/A-006 194

SEISMIC DISCRIMINATION

Michael A. Chinnery

Massachusetts Institute of Technology

Prepared for:

Electronic Systems Division
Advanced Research Projects Agency

31 December 1974

DISTRIBUTED BY:

NTIS

National Technical Information Service
U. S. DEPARTMENT OF COMMERCE

Reproduced by
NATIONAL TECHNICAL
INFORMATION SERVICE
US Department of Commerce
Springfield, VA. 22151

UNCLASSIFIED

SECURITY CLASSIFICATION OF THIS PAGE *(When Data Entered)*

REPORT DOCUMENTATION PAGE		READ INSTRUCTIONS BEFORE COMPLETING FORM
1. REPORT NUMBER ESD-TR-74-344	2. GOVT ACCESSION NO.	3. RECIPIENT'S CATALOG NUMBER AD/A-006194
4. TITLE *(and Subtitle)* Seismic Discrimination		5. TYPE OF REPORT & PERIOD COVERED Semiannual Technical Summary, 1 July – 31 December 1974 6. PERFORMING ORG. REPORT NUMBER
7. AUTHOR*(s)* Chinnery, Michael A.		8. CONTRACT OR GRANT NUMBER*(s)* F19628-73-C-0002
9. PERFORMING ORGANIZATION NAME AND ADDRESS Lincoln Laboratory, M.I.T. P.O. Box 73 Lexington, MA 02173		10. PROGRAM ELEMENT, PROJECT, TASK AREA & WORK UNIT NUMBERS ARPA Order 512
11. CONTROLLING OFFICE NAME AND ADDRESS Advanced Research Projects Agency 1400 Wilson Boulevard Arlington, VA 22209		12. REPORT DATE 31 December 1974 13. NUMBER OF PAGES 63
14. MONITORING AGENCY NAME & ADDRESS *(if different from Controlling Office)* Electronic Systems Division Hanscom Air Force Base Bedford, MA 01731		15. SECURITY CLASS. *(of this report)* Unclassified 15a. DECLASSIFICATION DOWNGRADING SCHEDULE

16. DISTRIBUTION STATEMENT *(of this Report)*

Approved for public release; distribution unlimited.

17. DISTRIBUTION STATEMENT *(of the abstract entered in Block 20, if different from Report)*

18. SUPPLEMENTARY NOTES

None

Reproduced by
NATIONAL TECHNICAL INFORMATION SERVICE
US Department of Commerce
Springfield, VA 22151

PRICES SUBJECT TO CHANGE

19. KEY WORDS *(Continue on reverse side if necessary and identify by block number)*

seismic discrimination	surface waves	NORSAR
seismic array	LASA	ARPANET
seismology	body waves	

20. ABSTRACT *(Continue on reverse side if necessary and identify by block number)*

This report describes 22 separate investigations in the field of seismic discrimination. These are grouped as follows: Discrimination and evasion research (5 contributions), method for the determination of focal depth (4 contributions), global seismic network studies (4 contributions), studies of earth heterogeneity (4 contributions), source mechanism studies (3 contributions), and investigations of global seismic activity (2 contributions).

DD FORM 1 JAN 73 1473 EDITION OF 1 NOV 65 IS OBSOLETE

UNCLASSIFIED

SECURITY CLASSIFICATION OF THIS PAGE *(When Data Entered)*

MASSACHUSETTS INSTITUTE OF TECHNOLOGY
LINCOLN LABORATORY

SEISMIC DISCRIMINATION

SEMIANNUAL TECHNICAL SUMMARY REPORT
TO THE
ADVANCED RESEARCH PROJECTS AGENCY

1 JULY – 31 DECEMBER 1974

ISSUED 28 JANUARY 1975

Approved for public release; distribution unlimited.

LEXINGTON MASSACHUSETTS

ABSTRACT

This report describes 22 separate investigations in the field of seismic discrimination. These are grouped as follows: Discrimination and evasion research (5 contributions), method for the determination of focal depth (4 contributions), global seismic network studies (4 contributions), studies of earth heterogeneity (4 contributions), source mechanism studies (3 contributions), and investigations of global seismic activity (2 contributions).

CONTENTS

Preceding page blank

SUMMARY

This is the twenty-se annual Technical Summary report describing the activities of Lincoln Laborator[illegible] ne field of seismic discrim nation. These activities involve research into the fundamental seismological problems associated with the detection, location, and identification of earthquakes and nuclear explosions. We are also concerned with the development of methods for the handling and analysis of large quantities of global seismic data, both from the point of view of data management system design, and also to facilitate the optimum extraction of scientific information from high-quality digital data.

Research into topics directly related to seismic discrimination and evasion has concentrated on two areas. First, some new approaches to the determination of surface wave magnitude are described. It is shown that useful information about the shape of the group velocity curve can be deduced directly from the seismogram, and this leads to a much more satisfactory path correction than those commonly employed. Second, we are exploring multivariate techniques that will enable a much more complete parametric representation of the seismogram to be applied to the problems of discrimination and evasion. Current research includes the simultaneous application of multiple discriminants, discrimination between different source mechanisms, and an approach to the multiple shot evasion problem.

A number of studies of methods for the determination of focal depth are described. Very promising results are shown for the identification of the surface reflection pP from explosions using maximum entropy cepstral analysis. This technique has the potential for becoming a powerful tool in any seismic monitoring scheme. Continued study of the effect of depth on surface wave spectra shows a strong influence of crustal structure, enough to make the method somewhat suspect. Application of measurements of S-P times is discussed, and, although the method is potentially powerful, there is clearly considerable difficulty in identifying the S arrival in many instances. Another study attempts to model the characteristics of the proposed DARPA seismic network. It is shown that this network will have some difficulty in resolving accurate focal depths for many events in Eurasia.

We are continuing our work on the development of a management structure for data and information from the proposed DARPA seismic network. Application of the NLS system, developed by Stanford Research Institute, appears promising, and experiments in the storage and retrieval of information via the ARPANET are being carried out. Other network studies include a continuation of our effort during the International Seismic Month, with emphasis on the characteristics of a 32-station network. With careful data analysis, it appears that such a network is almost as good as the whole set of ISM stations for the production of a global earthquake bulletin.

Our studies of the nature of inhomogeneity in the earth are becoming heavily involved in scattering processes, particularly in the mantle. Several investigations described in this report indicate that these processes may play a dominant role in the absorption and conversion of energy in short-period body waves. The presence of anisotropy in the scattering medium is postulated, and is shown to constitute a potentially important effect.

In the field of seismic source mechanisms, we describe several studies aimed at the interpretation of source parameters from observations of long-period body and surface waves. One study indicates the possibility of determining gross source characteristics from long-period P-waves. Another describes a method for the estimation of source parameters from the amplitude and phase spectra of surface waves from pairs of earthquakes.

Preceding page blank

We have also initiated a study of the time variation of seismic activity, hoping to clarify problems related to network detection and hide-in-earthquake evasion. Evidence is shown that the level of global seismic activity shows rapid fluctuations in level that are largely independent of magnitude. Viewed as a time series, the activity variations appear to contain some significant periodicities, though the cause of these has yet to be established.

In anticipation that digital seismic data soon will be available in quantity on the ARPANET, we are continuing to develop a facility to enable us to access and manipulate these data. We are presently in the process of developing the necessary software, and we anticipate being able to access this new information source when it becomes available.

M. A. Chinnery

GLOSSARY

AEC	Atomic Energy Commission
ARPANET	ARPA Computer Network
BME	Burg Maximum Entropy (spectrum)
DARPA	Defense Advanced Research Projects Agency
FFT	Fast Fourier Transform
ISC	International Seismological Center
ISM	International Seismic Month
IWWSS	Integrated World-Wide Seismic System
LASA	Large Aperture Seismic Array
m_b	Body Wave Magnitude
M_s	Surface Wave Magnitude
NEIS	National Earthquake Information Service
OLS	On-Line System
NORSAR	Norwegian Seismic Array
NTS	Nevada Test Site
PDE	Preliminary Determination of Epicenter
SATS	Semiannual Technical Summary
SRO	Seismic Research Observatory
USCGS	United States Coast and Geodetic Survey
USGS	United States Geological Survey
WWSSN	World-Wide Standard Seismograph Network

SEISMIC DISCRIMINATION

I. DISCRIMINATION AND EVASION

A. M_s:m_b FOR EARTHQUAKES WITH COMPLEX SHORT-PERIOD WAVEFORMS

It has been shown[1] that, by firing an ordered sequence of explosions, the complexity and M_s:m_b ratio of an earthquake may be mimicked. It is reasonable to conjecture, however, that the complexity of the short-period waveform and the level of long-period energy contained in the surface waves are both due to the source mechanism. The result would be that earthquakes of a given M_s:m_b ratio would have a characteristic short-period waveform as well. To investigate this hypothesis, earthquakes from the linear region of shallow focus seismicity just north of the Hindu Kush were divided into two classes based on the emergent or impulsive characteristic of the first 15 sec of their short-period teleseismic P-waveforms, and their M_s:m_b ratios were computed. Figure I-1 shows typical waveforms of the two classes and a synthetic seismogram produced by the superposition of a P-waveform of an explosion. Due to the constructive interference of the surface waves and the use of an initially small explosion, the M_s will increase by approximately 0.5 and the m_b will decrease by approximately 0.5 for the multiple explosion compared with that of a single explosion. Such behavior is illustrated in Fig. I-2 where the box labeled A represents the spread of M_s:m_b at m_b = 5.75 for presumed Eastern Kazakh explosions,[2] and the box labeled B represents the expected M_s:m_b region in the earthquake population that the multiple explosion would fall into. The points marked with an X are for Class 2 (impulsive) earthquakes, while those marked with an O represent Class 1 (emergent) earthquakes. The trend line for M_s:m_b for this region[2] shown in the figure is also the line that separates the two classes of short-period waveforms. While the multiple event M_s:m_b is earthquake-like, its waveform (Class 1) is not characteristic of events with comparable M_s:m_b values.

The purpose of this study was not to show that multiple-event evasion is not possible, but rather that under any evasion scheme the total character of both the long- and short-period seismic energy must be considered.

T. E. Landers
R. E. Needham

B. SURFACE WAVE MAGNITUDE PATH CORRECTION

During the computation of surface wave magnitudes (M_s) for the International Seismic Month (ISM) events, it became clear that appropriate path and period corrections were necessary when using globally distributed stations with various response characteristics. In the ISM long-period study, M_s path corrections given as a function of period by Marshall and Basham[2] were applied. Although these corrections represent a significant advance in reducing the variance in an M_s determination from a network of stations, they are cumbersome to apply in any automatic processing scheme. The difficulties lie in determining the nature of the path of any given surface wave ray and the magnitude of the path correction along paths not studied by Marshall and Basham. As these authors correctly point out, the path correction, as a function of period, depends chiefly upon the slope of the group velocity curve between the epicenter and each recording station. The suggestion is made here that, in some cases, this slope can be directly from the seismogram and a path correction, which is in a sense optimum, may be computed for each individual amplitude measurement.

It has been shown by Ben-Menahem and Jeffreys[3] and others that the amplitude of fundamental mode surface waves of a given frequency (ω_o) may be approximated in the time domain by

$$A(t,\Delta) = \frac{L_o}{(\sin\Delta)^{1/2}} A(\omega_o) \exp\left[(-\omega_o t/2Q)\left(\frac{2\pi}{t|\omega_o''|}\right)^{1/2}\right] \qquad (I\text{-}1)$$

where Δ is the epicentral distance in degrees, L_o is the source radiation effect, $A(\omega_o)$ is the source spectral amplitude at ω_o, Q is a dimensionless attenuation parameter, and ω_o'' is the second derivative of ω with respect to wave number k at ω_o. In Eq. (I-1), the parameters that determine the source strength or magnitude at a given azimuth and frequency are L_o and $A(\omega_o)$. The other terms are path effects for which we would like to correct. If we assume that the epicentral distance, the travel time, and the surface wave attenuation parameter are known, then the only remaining correction, the path correction, is proportional to $(t|\, d^2\omega/ak^2|_o)^{1/2}$. It may be shown that this factor, in terms of quantities that can be directly measured on the seismogram, may be approximated by

$$\left(t\left|\frac{d^2\omega}{dk^2}\right|_o\right)^{1/2} \approx \Delta \frac{T_o}{t} \left(\frac{\delta t}{\delta T}\right)^{1/2} .$$

Here, T_o is the period (in seconds) of the particular phase where magnitude is being measured, t is travel time (in seconds), δt is the difference in arrival time of the preceding and succeeding phases, and δT is the difference in the period of these phases. Again, the latter two differences may, in some cases, be measured directly on the seismogram and they allow the reader to account for the path dispersion effects in a manner that is relevant to that seismogram.

An example of the method is shown in Fig. I-3. The data trace in this figure represents the vertical component of the Rayleigh wave recorded at the World-Wide Standard Seismograph Network (WWSSN) station at Valentia, Ireland from a Novaya Zemlya explosion. The triangles on the lower plot represent M_s units measured by the conventional term $\log_{10}(A/T)$ at the numbered phases of the seismogram. The open circles represent the term $\log_{10}(A)$ plus a path correction computed as suggested above. In both cases, the measurements of amplitude (A) were corrected for the frequency response of the WWSSN long-period instruments. It may be seen in Fig. I-3 that, in this case, the suggested method for path correction gives a more stable M_s measurement over a wide-period range than the conventional method. A test of the suggested method on a large data population is being undertaken. The method will not apply if multipath propagation is evident on the long-period seismogram, but a few M_s measurements made by the new method may prove more reliable than many measurements made on complicated seismograms.

An alternative method for estimating the slope of the group velocity curve is described in the following contribution.

J. R. Filson

C. AUTOMATIC AND CONTINUOUS MEASUREMENT OF AMPLITUDE AND FREQUENCY

As reported elsewhere in this SATS, a new way of measuring surface wave magnitudes is being developed. This method requires that the slope of the group velocity curve as well as the amplitude and frequency of the arriving signal be measured. In fact, if instantaneous frequency and amplitude can be measured as a function of time for a surface wave, the method allows one

to measure M_s over the complete range of arriving frequencies. We have started to investigate a method by which such measurements can be made automatically by a computer.

A dispersed Rayleigh wave can be approximated by

$$s(t) = A(t) \cos[\theta(t)]$$

where A(t) is the envelope of the signal and

$$w(t) = \frac{d}{dt}\,\theta(t)$$

is the instantaneous radian frequency. If neither w(t) nor A(t) change too quickly with time, there is a way to extract A(t) and w(t) which is quite convenient to realize automatically on a computer. Given w(t), A(t) is the amplitude required to measure M_s at that frequency. Since we have w(t), the origin time, and the distance of the event, we can also obtain the required group velocity curve. Thus, the time functions w(t) and A(t) will allow us to obtain a time function $M_s(t)$. The value of this time function at time t will be an M_s value for frequency $w(t)/2\pi$.

The method uses the complex analytic representation

$$\tilde{s}(t) = s(t) + i\bar{s}(t)$$

where $\bar{s}(t)$ is the Hilbert transform of the real signal s(t). The Hilbert transform can be realized either by a time domain filter or by application of a 90° phase shift in the frequency domain. Both methods are being tried, although the data shown below were obtained using the frequency domain approach. The functions A(t) and w(t) are obtained from $\tilde{s}(t)$ by

$$A(t) = \sqrt{\tilde{s}(t)\,\tilde{s}^*(t)}$$

and

$$w(t) = \frac{d}{dt}\,\mathrm{Im}\,\{\ln \tilde{s}(t)\}$$

where Im denotes taking the imaginary part of the complex logarithm.

Figure I-4 shows a seismogram, the envelope A(t), and the frequency $w(t)/2\pi$ obtained from it. Time differentiation to obtain w(t) is just a scaled first difference of adjacent data points, and we plan to consider better algorithms which will not give such a noisy output. The very top and bottom traces are A(t) and $w(t)/2\pi$ filtered by a low-pass filter with a corner frequency of 0.02 Hz.

This effort to automatically and continuously measure amplitude and frequency is just getting under way. The initial results are encouraging. We plan now to improve our programs and combine them with algorithms for measuring M_s. The computer load to extract A(t), w(t) is not excessive and is about equivalent to filtering with a 50-point convolutional filter.

R. T. Lacoss

D. APPLICATION OF PATTERN RECOGNITION TO SEISMIC DISCRIMINATION

In the past four years, there has been a revival of interest in short-period discrimination of explosions and earthquakes, particularly at low magnitudes for which surface wave measurements cannot be made. Anglin[4] demonstrated that explosions and shallow earthquakes in Eurasia, recorded at the Yellowknife array, could be separated on a plot of complexity vs third moment of frequency, whereas if either parameter were used alone, there was considerable

overlap between the explosion and earthquake populations. Further studies[5-7] verified the value of multiple discriminants and even multisite studies, although it has become clear that careful regional studies of spectral parameters must be made.[8]

We are attempting to apply some techniques of pattern recognition to the discrimination problem. The method of Fukunaga and Koontz[9] is promising because it is designed to extract discriminating features for two classes of data. Briefly, the technique assumes that n parameters have been measured for each event of two distinct classes. For each event, the various parameters are elements x_i of a data vector

$$\overline{X} = \text{col}\,(x_1, x_2, \ldots, x_n) \quad . \tag{I-2}$$

For each class, the autocorrelation matrix

$$R_i = E_i\{\overline{X}\overline{X}^T\} \quad , \quad i = 1, 2 \tag{I-3}$$

is estimated, where E_i is the expectation of Class i data. A "mixture" R_o of the two classes is defined as the sum of the two autocorrelation matrices, i.e.,

$$R_o = R_1 + R_2 \quad . \tag{I-4}$$

The next step is to determine a coordinate transformation Γ which diagonalizes and whitens R_o. Applying this to R_o, we obtain

$$I = S_1 + S_2 \tag{I-5}$$

where

$$S_i = PR_iP^T \quad , \quad i = 1, 2 \quad . \tag{I-6}$$

From Eq. (I-5), it can be shown that S_1 and S_2 have the same set of eigenvectors, and for each eigenvector the eigenvalues of S_1 and S_2 are related by

$$\lambda_1 = 1 - \lambda_2 \tag{I-7}$$

where $1 \geq \lambda_i \geq 0$. If λ_1 is the largest eigenvalue, e.g., nearly unity, then λ_2 is almost 0, so that the eigenvector with these eigenvalues is the most important feature or basis vector of Class 1 data, while simultaneously being the least-significant feature of Class 2 data.

Projecting the data vectors of each class onto the eigenvectors with eigenvalues near 1 or 0 should give the best separation of the two classes. By assuming a normal distribution of each data class as projected onto these eigenvectors, the crossover point and misidentification probabilities can be determined. That eigenvector which gives the smallest misidentification probability is therefore the direction along which the class separation is best.

To illustrate this technique, an experiment was run using 11 Central Asian earthquakes and 12 presumed explosions in Eastern Kazakh. The earthquakes, taken to be the first class of events, are from the Kirgiz-Sinkiang border region, Tadzhik-Sinkiang border region, and southern Sinkiang, all within about 10° distance from the concentration of Eastern Kazakh events, which form Class 2 data. The data used were recorded at NORSAR, and the parameters investigated were m_b, log third moment of the spectrum (LTM), complexity (CMPLX), and M_s.

The significant short-period parameters are LTM and complexity, which are plotted in Fig. I-5 for the two classes of data. The LTM values were obtained by Noponen[8] by

spectraforming the NORSAR subarray beams of each event. This method of estimating short-period-event spectra is designed to preserve the high frequencies usually lost in conventional beamforming. The complexity values were obtained using the quadratic complexity formula of Kelly[10] with an additional correction for noise power.

The separation of the two classes is very clear, although either discrimination parameter alone does not give perfect separation. Figure I-6 shows an M_s vs m_b plot for the events of Fig. I-5 which had NORSAR M_s values measured. As in Fig. I-5, the separation is perfect.

Using these data, the Fukunaga-Koontz method described above was applied to the two classes of events. The results are summarized in Table I-1. In each case, the parameters used in the data vectors are marked by x's.

TABLE I-1
PATTERN RECOGNITION USING CENTRAL ASIAN EARTHQUAKES (Q) AND PRESUMED EXPLOSIONS (EX)

Case	No. of Events		Parameters					Probability of Errors (percent)
	Q	EX	m_b	LTM	CMPLX	M_s	m_b-M_s	
1	11	12	x	x	x			6
2	11	12		x	x			5
3	7	10	x			x		0
4	7	10		x	x			6
5	7	10		x			x	0
6	7	10			x		x	0

For the first two cases, all events of each class were used. By using only short-period discriminants the probability of misclassification is ~5 or 6 percent. The error is reduced slightly by using LTM and CMPLX without m_b, because m_b is not correlated with the other parameters and simply adds noise to the problem. Cases 3 to 6 utilize the data for which NORSAR M_s values were available. As to be expected, parameters M_s and m_b produce the smallest probability of error, essentially 0 in Case 3. In Case 4, the short-period discriminants for the same event yield an error probability of 6 percent. Finally, Cases 5 and 6 combine (m_b-M_s) with a single short-period discriminant. Again, the overwhelming effect of the parameter (m_b-M_s) causes the probability of error to vanish.

Because the two classes of events are small, the statistics given in these examples are unreliable. This is likely to remain a serious problem if only short-period parameters are used. Strong variations in the tectonics and attenuation across Asia[8] imply that data must be carefully studied in small regions. Clearly, difficulties in separation will occur at lower m_b when detection and noise problems become severe.

The best way to stabilize the statistics for small classes is to use several recording sites. This requires an adaptation of pattern-recognition techniques to multistation data, which is now being investigated for a wide range of magnitudes.

C. W. Frasier
A. Shakal

E. DISCRIMINATION BETWEEN SOURCE MECHANISMS

A study of the feasibility of discriminating among source mechanisms of mid-ocean ridge earthquakes is under way. Since earthquakes in the mid-ocean ridge systems have principally either normal (on the ridge proper) or strike-slip (on transform faults) source mechanisms,[11] discrimination between these two types will be attempted using the modified Karhunen-Loeve expansion of Fukunaga and Koontz[9] as discussed above. Events of the central Mid-Atlantic Ridge are being studied by the analysis of single-station signals, the station being the LASA or NORSAR array.

Data from earthquakes with epicenters near earthquakes with previously determined focal mechanisms[11-13] form the observation vectors of the training set for the recognition algorithm. The measurements making up these observation vectors include those frequently used in earthquake-explosion discrimination studies, as above. In addition, other discriminants which might be more appropriate for this problem are being considered. Hopefully, information might be obtained from this study to allow a better understanding of the wide variation seen in typical M_s-m_b plots and to infer how much of this might be due to real effects of the mechanism of the source.

Certain tentative results suggest themselves from preliminary analysis. First, it appears that the separability of these two populations is not as good as in the earthquake-shot populations. Thus, the level of correct separation will not be as high at similar magnitudes. Secondly, it appears that ridge earthquakes have more similarity among themselves than do transform earthquakes. However, further analysis of more data will be necessary before solid conclusions can be made.

A. Shakal

REFERENCES

1. Seismic Discrimination SATS, Lincoln Laboratory, M.I.T. (30 June 1973), DDC AD-766559/9.
2. P. D. Marshall and P. W. Basham, "Discrimination Between Earthquakes and Underground Explosions Employing an Improved M_s Scale," Geophys. J. R. Astr. Soc. 28, 431-458 (1972).
3. A. Ben-Menahem and H. Jeffreys, "Saddle Point Approximation for Damped Surface Waves," Geophys. J. R. Astr. Soc. 24, 1-2 (1971).
4. F. M. Anglin, "Discrimination of Earthquakes and Explosions using Short-Period Seismic Array Data," Nature 233, 51-52 (1971).
5. H. Israelson, "Seismic Identification using Short Period Hagfors Data," Proc. Semin. Seismology and Seismic Arrays, NTNF/NORSAR, 66-78, 30 September 1972.
6. F. M. Anglin and H. Israelson, "Seismological Discrimination of Earthquakes and Explosions using Multistation Short-Period Data," Bull. Seismol. Soc. Am. 63, 321-323 (1973).
7. H. Israelson, "Short Period Identification," draft of paper given at the NATO Advanced Study Institute on Exploitation of Seismograph Networks, Sandefjord, Norway, 22 April – 3 May 1974.
8. I. Noponen, "Compressional Wave Power Spectrum from Seismic Sources," Scientific Report No. 1, Institute of Seismology, University of Helsinki (31 October 1973).
9. K. Fukunaga and W. L. Koontz, "Application of the Karhunen-Loeve Expansion to Feature Selection and Ordering," IEEE Trans. Computers C-19, 311-318 (1970).

10. E. J. Kelly, "A Study of Two Short-Period Discriminants," Technical Note 1968-8, Lincoln Laboratory, M.I.T. (12 February 1968), DDC AD-666701.

11. L. R. Sykes, "Mechanism of Earthquakes and Nature of Faulting on the Mid-Oceanic Ridges," J. Geophys. Res. 72, 2131-2153 (1967).

12. L. R. Sykes, "Focal Mechanism Solutions for Earthquakes Along the World Rift System," Bull. Seismol. Soc. Am. 60, 1749-1752 (1970).

13. D. J. Weidner and K. Aki, "Focal Depth and Mechanism of Mid-Ocean Ridge Earthquakes," J. Geophys. Res. 78, 1818-1831 (1973).

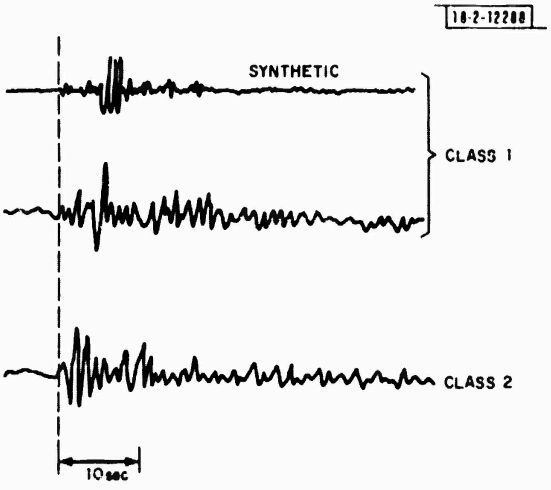

Fig. I-1. Typical short-period P-waves for two classes of events. Class 1 is emergent; Class 2 is impulsive.

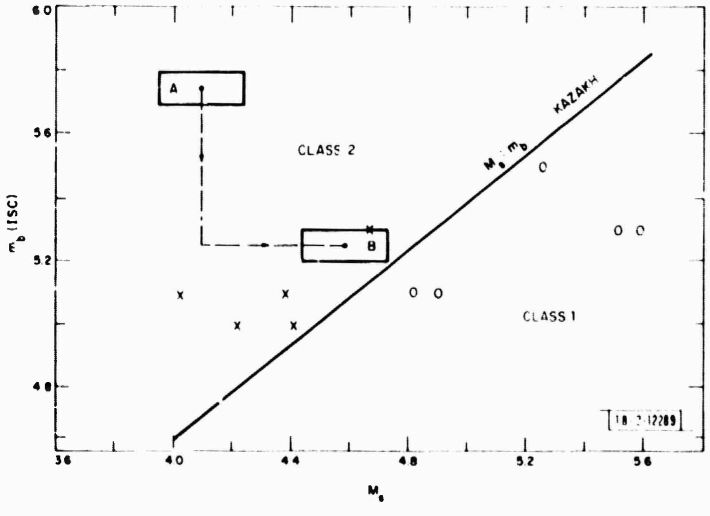

Fig. I-2. M_S:m_b for Class 1 (emergent) events O and Class 2 (impulsive) events X. Multiple explosion M_S:m_b would fall into box B from single explosion region, box A. Its short-period record is, however, Class 1. Solid line is trend for all Kazakh earthquakes.[2]

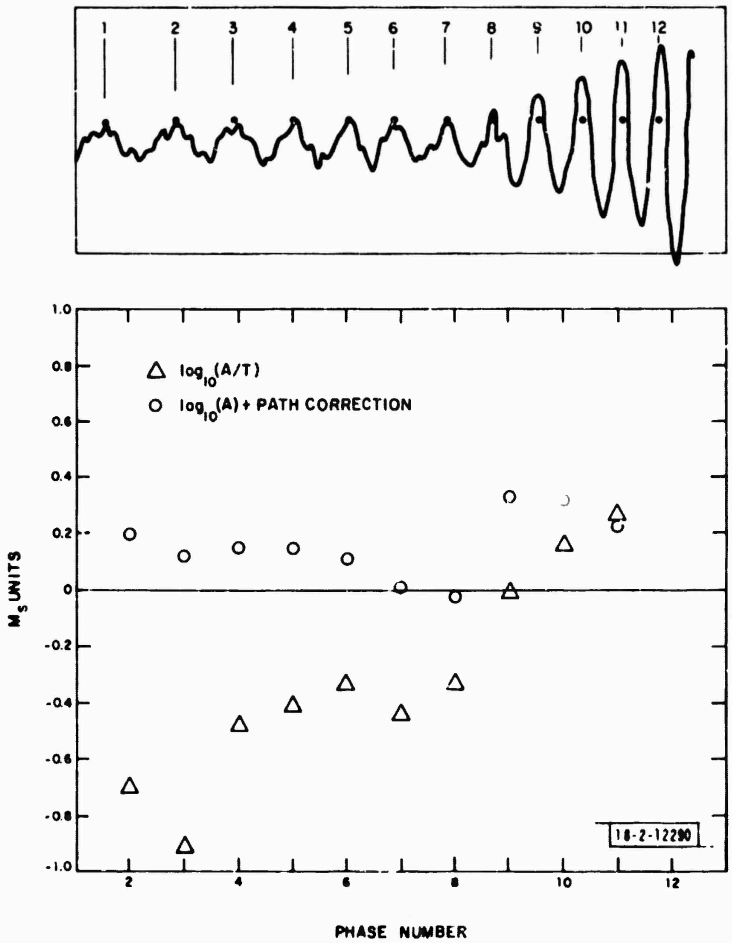

Fig. I-3. Comparison of conventional and suggested methods for computing M_S.

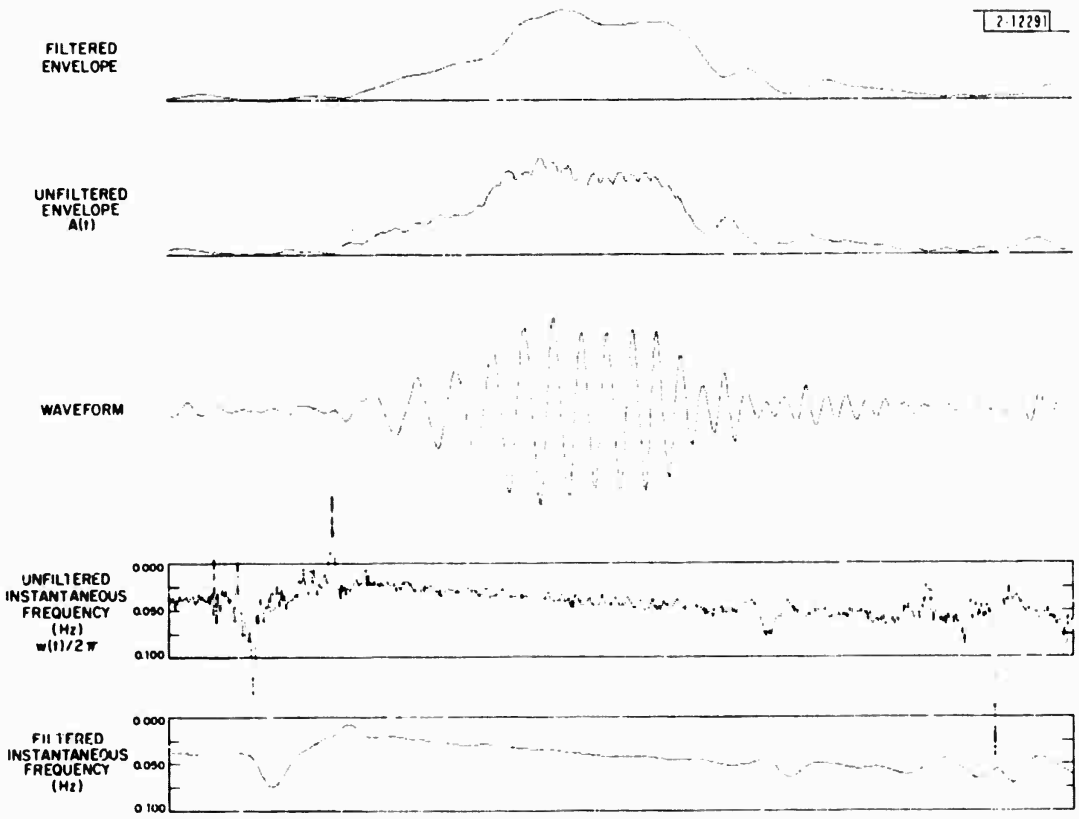

Fig. I-4. Example of extraction of instantaneous amplitude and frequency of surface wave by means of discrete Hilbert transform.

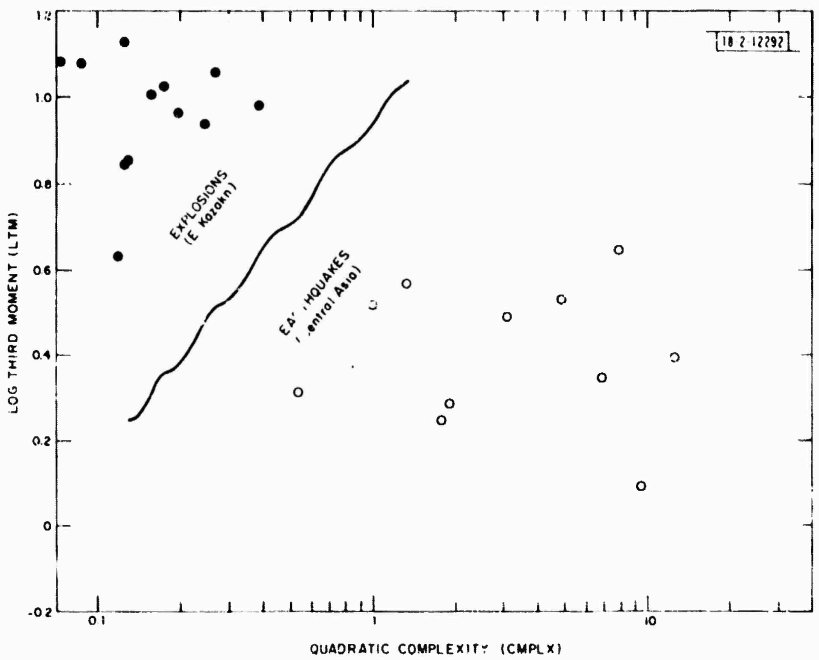

Fig. I-5. Separation of presumed explosions in Eastern Kazakh from nearby Central Asian earthquakes using LTM and quadratic CMPLX.

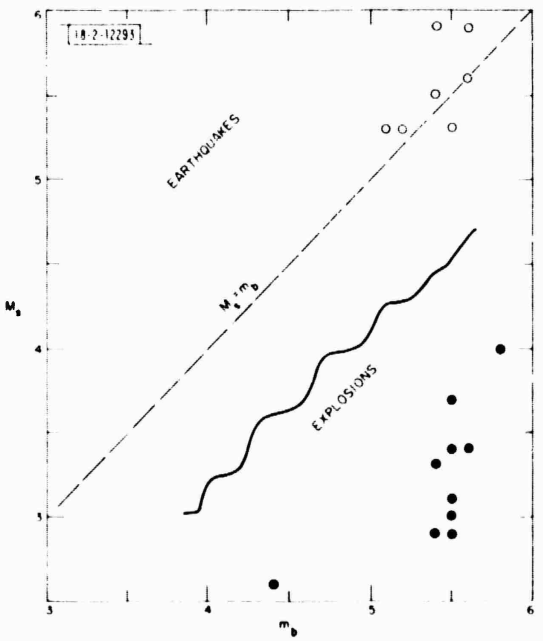

Fig. I-6. Separation of those events of Fig. I-5 which have measured NORSAR M_S values.

II. FOCAL DEPTH

A. FOCAL DEPTH RESOLUTION USING THE DARPA SEISMIC NETWORK

Preliminary theoretical studies have been made of the expected accuracy with which seismic event locations will be determinable by the DARPA seismic network. Other calculations of this same general sort have been reported in a previous SATS.[1] Estimates of the probable errors contaminating arrival time measurements are mapped into estimates of the probable errors in derived hypocentral parameters.

For the purpose of these calculations, stations which are not yet installed were represented by existing stations located nearby. Twelve short-period stations, including both arrays and seismic research observatories (SROs) whose locations are known, were used:

LASA	
NORSAR	
SEO	Seoul, Korea (representing the Korean array)
MSH	Mashed, Iran (representing the Iranian array and SRO)
ANK	Ankara, Turkey (SRO)
SHL	Shillong, India (SRO)
WEL	Wellington, New Zealand (SRO)
ANP	Anpu, Taiwan (SRO)
ALQ	Albuquerque, New Mexico (SRO)
BOG	Bogota, Colombia (SRO)
GUA	Guam, Mariana Islands (SRO)
AAE	Addis Ababba, Ethiopia (SRO)

Figures II-1(a) and (b) show the expected standard error of focal depth calculated on the assumption that P-waves are detected by all stations within 95° of an event and that the arrival times have standard errors of 1.0 sec (including the combined effects of reading errors, clock errors, etc., and variations between actual travel times for various paths and the travel time tables used). From these figures, it appears that the network may not be able to resolve focal depth well enough to make it a useful discriminant for most shallow earthquakes in Asia.

B. R. Julian

B. DETECTING THE DEPTH PHASE OF EXPLOSIONS

Cepstral analysis, using the Burg Maximum Entropy (BME) method to estimate the spectrum of the log spectrum (quefrency), has been used to determine the arrival time of the depth phase in NTS explosions recorded in Norway ($\Delta \approx 70°$). The technique was described and applied to synthetic data in the last SATS.[2] By using the high-resolution BME method, it is possible to make accurate spectral estimates on the complex quefrency when the echo delay time is small and when only that part of the quefrency that contains significant power is used. Figures II-2 through II-5 illustrate the usefulness of this technique.

Figure II-2 shows the short-period P-wave of Boxcar recorded at Oyer and the tapered version used in this analysis. The amplitude and phase components of the spectrum are presented in the top half of Fig. II-3. Initially, the band 0.3 to 2 sec was chosen. Removing the effect of the instrument and attenuation ($t^* = 0.25$), the linear trend in the phase (a time delay) and the

linear trend in the log amplitude (a source correction), and using the window 0.5 to 2 Hz results in the complex quefrency shown in the bottom half of Fig. II-3. Figure II-4 shows the Burg prediction error filter designed on the complex quefrency, and Fig. II-5 depicts the cepstrum obtained from that filter. The peak at 0.88 sec is interpreted as the delay time between the P-wave and pP. Springer[3] reports a pP-P time of 0.96 sec for Boxcar using surface zero accelerometer records. The difference amounts to 1 digitizing unit. The delay time is plotted in Fig. II-2 on the original seismogram, and the peak at 2 sec in the cepstrum is also displayed as a time delay. Springer[3] reports a surface spall closure at 3.07 sec for this event. The delay time of 2 sec found here is consistent with the short-period waveform and may indicate that it is not necessarily the surface spall closure that produces teleseismic energy.

Similar results have been found for other NTS explosions recorded in Norway. The shortest echo delay times found so far have been approximately 0.6 sec. It seems possible that this technique will be useful down to delay times as short as a few tenths of a second on data sampled at 20 Hz.

T. E. Landers

C. CRUSTAL FOCAL DEPTH DETERMINATIONS FROM SURFACE WAVES

In the last SATS,[2] it was shown that variations in upper-mantle shear velocity, particularly the existence of thin high-velocity layers, seriously affect the accuracy of depth determinations from Rayleigh-wave spectra. This study has been extended to include the effects of crustal structure variations, where, of course, thin high-velocity layers may also exist. So far, source spectra have been computed for three different shield models – the Canadian Shield,[4] and Baltic and West Siberian Shields,[5] where the upper-mantle structure has been assumed to be the same for all three. The dispersion curves for these are identical to within 0.05 km/sec in the period range 20 sec upward.

Spectra at a range of depths for various fault orientations have been calculated within one of these models, and a search then was conducted over depth for the best fitting spectra of the other models – a method identical with that used in recent studies[6,7] except that the observational spectra have been replaced by theoretical spectra for the first model. Both phase and amplitude spectra have been fitted separately; for the latter, the absolute level of the spectrum, governed by the seismic moment, has been determined within the fitting scheme both from the amplitude ratio at long periods and from the average over the whole period range considered (16 to 60 sec).

It has been found, as expected, that source spectra with distinctive features such as "holes" or sharp phase changes can be fitted better than those without such discontinuities. When the source is at depths too shallow for these to appear within the period range used, the phase resolution is very poor. Tests with a variety of fault orientations reveal no general rule concerning the relative resolution or accuracy of phase and amplitude spectra in depth determination. Figure II-6 illustrates a case where the phase gives a much sharper fit than amplitude; sometimes the reverse is true. Fitting phase and amplitude simultaneously does not seem to improve the situation.

Figure II-7 shows the depths at which the best fit was found for spectra for the Baltic shield, vs depths at which the fitted spectra were generated in the Canadian Shield, for a 45° dip-slip fault fitted at azimuths of 0, 30, . . . , 150°. For other fault models, the picture is generally the

same – the effect of the different earth models is most serious below 5 and above 25 km depth. It must be emphasized that, although this fit seems reasonable, the earth models used do not differ greatly and no errors in the fault orientation have been considered. This study is being extended to include the use of real instead of synthetic data.

R.G. North

D. S RESIDUALS VS DEPTH AT REGIONAL DISTANCES IN ASIA

We have begun to study the usefulness of the S-P interval in the problem of depth determination at near and regional distances. For this study, we have read the short-period recording at World-Wide Standard Seismographic Network (WWSSN) stations of some 300 Asian earthquakes. These events have all been located by the National Earthquake Information Service (NEIS) and reported in the Preliminary Determination of Epicenter (PDE) lists. The chief difficulty encountered so far is identifying the S arrival, which followed the same path as the initial P arrival, with an accuracy relevant to the determination of depth within a few kilometers at shallow depth. A second problem lies in establishing reliable S travel-time functions for the region of interest.

Figure II-8 shows a sample of the results obtained to date. Here, we have plotted S travel-time anomalies vs depth for 26 events located between 7° and 13° north of New Delhi, India (NDI). The anomalies (δ) are related to the S travel-time function, $T_c = 10.1 + (\Delta/4.72)$, given for India by Heustis, et al.,[8] and the observations (T_o) by $\delta = T_o - T_c$. The most discouraging aspect of Fig. II-8 is that the scatter of the data, over 100 km for a given δ, is much too great to be of use in accurate focal-depth determination. Assuming that the NEIS depths are accurate, most of this scatter must be due to our lack of ability to consistently identify the initial S arrival on the records read. A second disturbing feature of Fig. II-8 is that the S arrivals from near-surface sources in a restricted distance range to the north of NDI vary from 4 to 13 sec later than those predicted by Heustis, et al.[8] The latter used events located in the Himalayas and Burma to establish their S travel-time curve, while in the case of our readings at NDI the events were located in the Hindu Kush, Tadzhik, Kirgiz, and western Sinkiang. This indicates a strong path dependence on regional S velocities in Southern Asia.

An encouraging aspect of Fig. II-8 is that, despite our lack of experience in reading regional, short-period S arrivals, a definite trend with depth exists. This trend is not a function of distance since the events are well distributed at various depths in the distance range studied. Whether we can reduce the scatter through rereading the records and redefinition of the S travel-time function remains to be shown.

S. Das
M. T. Lin
J. R. Filson

REFERENCES

1. Seismic Discrimination SATS, Lincoln Laboratory, M.I.T. (31 December 1973), DDC AD-777151/2.
2. Ibid. (30 June 1974), DDC AD-785377/3.
3. D. L. Springer, "Secondary Sources of Seismic Waves from Underground Nuclear Explosions," Bull. Seismol. Soc. Am. 64, 581-594 (1974).
4. J. Brune and J. Dorman, "Seismic Waves and Earth Structure in the Canadian Shield," Bull. Seismol. Soc. Am. 53, 167 (1963).
5. Atlas of Asia and Eastern Europe, Vol. V., "Crust and Mantle Conditions," U. S. Geological Survey (1969).
6. D. J. Weidner and K. Aki, "Focal Depth and Mechanism of Mid-ocean Ridge Earthquakes," J. Geophys. Res. 78, 1818 (1973).
7. Y.-B. Tsai and W.-W. Shen, "Utility of Tsai's Method for Seismic Discrimination," Texas Instruments Report (30 November 1972).
8. S. Heustis, P. Molnar and J. Oliver, "Regional S_n Velocities and Shear Velocity in the Upper Mantle," Bull. Seismol. Soc. Am. 63, 269-475 (1973).

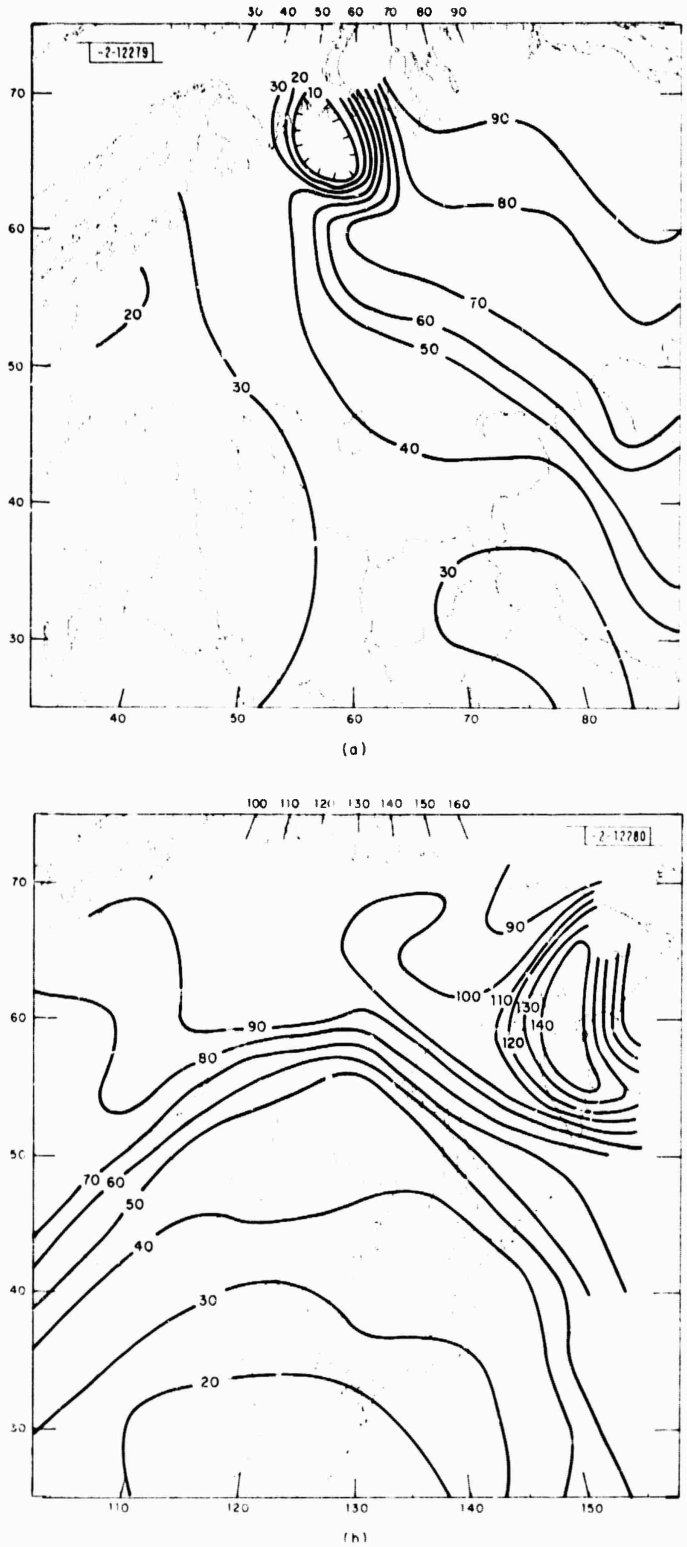

Fig. II-1. Standard error (km) of focal depths computed using P-waves only from DARPA seismic network assuming standard error of each arrival time of 1.0 sec. (a) Eastern half of Eurasia; (b) western half of Eurasia.

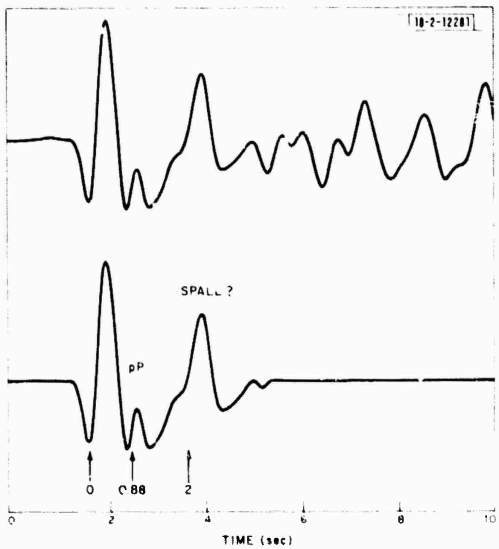

Fig. II-2. Boxcar as recorded at Oyer, and cosine tapered version used for analysis.

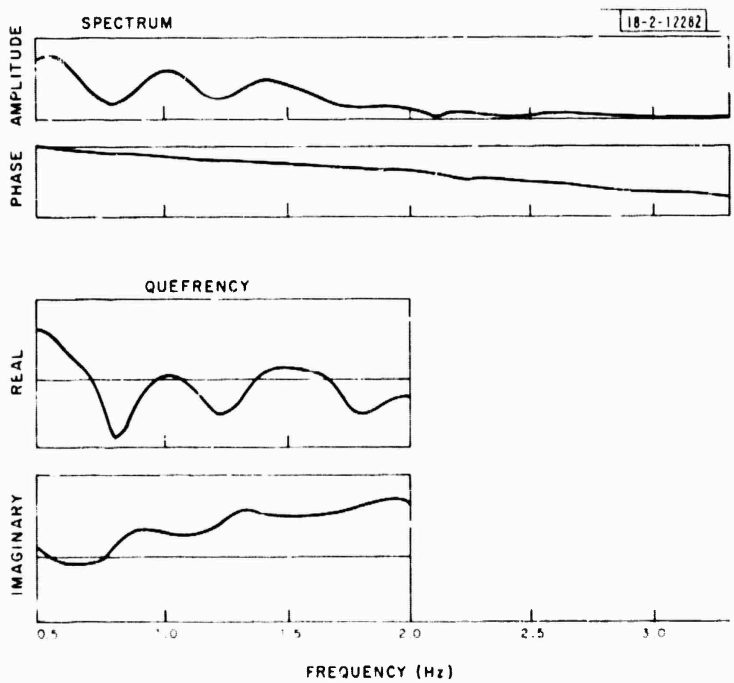

Fig. II-3. Spectrum and quefrency of Boxcar.

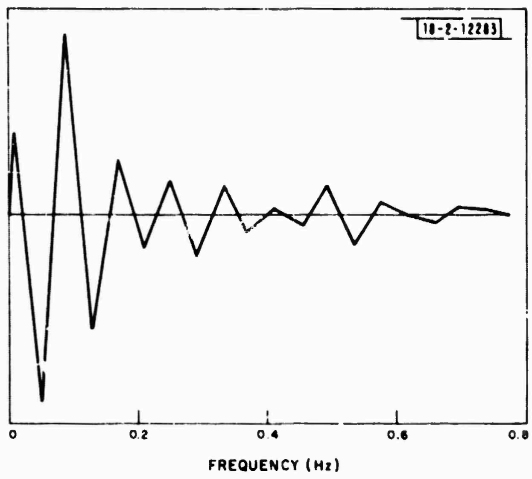

Fig. II-4. Burg prediction error filter designed on Boxcar's quefrency.

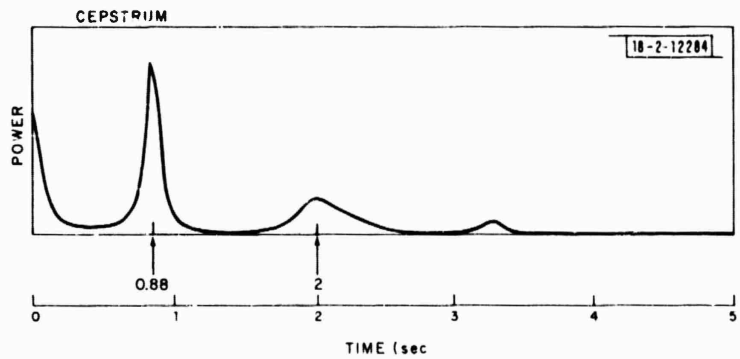

Fig. II-5. Cepstrum for Boxcar indicating that delay time for pP is 0.88 sec.

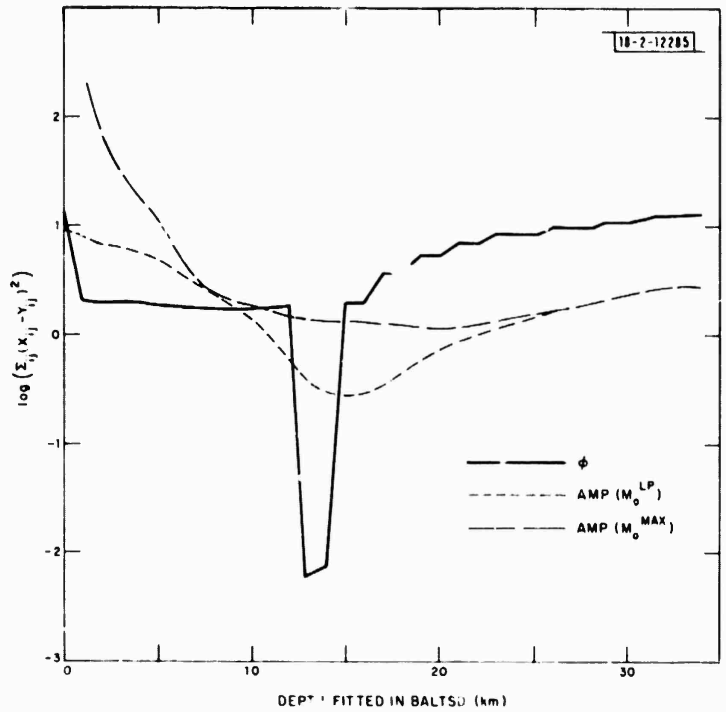

Fig. II-6. Fit [sum of squares of difference between spectra at 6 azimuths (0(30)150°) over period range 16 to 60 sec] of spectrum generated at 11 km depth in Canadian Shield model (CANSD) for strike-slip on 60° dipping plane to spectra in range 0 to 35 km for same fault within Baltic Shield (BALTSD). Minimum denotes best fit. Depths indicated by phase (φ), and amplitudes with moment determined by long-period spectral ratio [Amp (M_o^{LP})] and by averaging ratio over whole period range [Amp (M_o^{MAX})] are 13, 20, and 15 km, respectively. For this particular case, phase resolution is much better than that in amplitude.

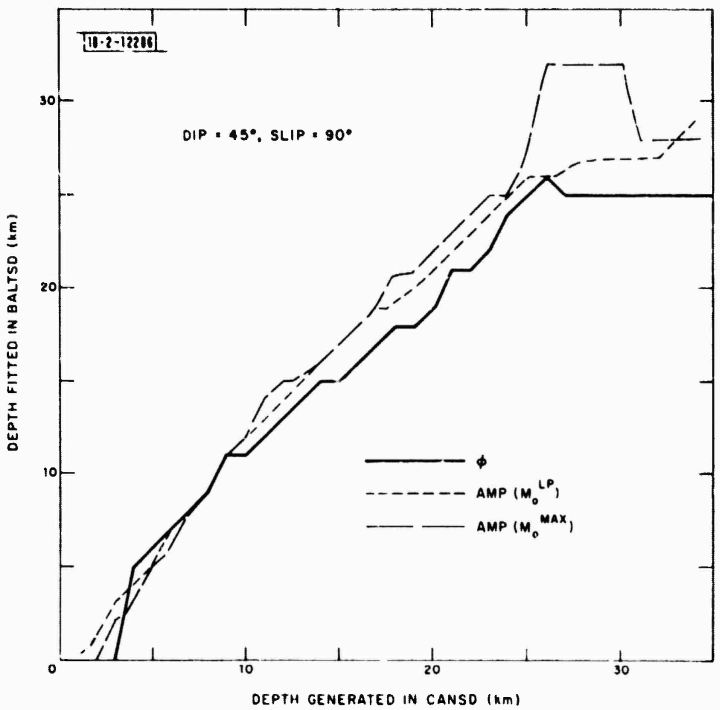

Fig. II-7. Best-fitting depths within BALTSD for spectra generated in CANSD for 45° dip-slip fault (pure thrust/normal fault) as function of depth. Depths given by all 3 fitting schemes are good except at very shallow depths and below 25 km.

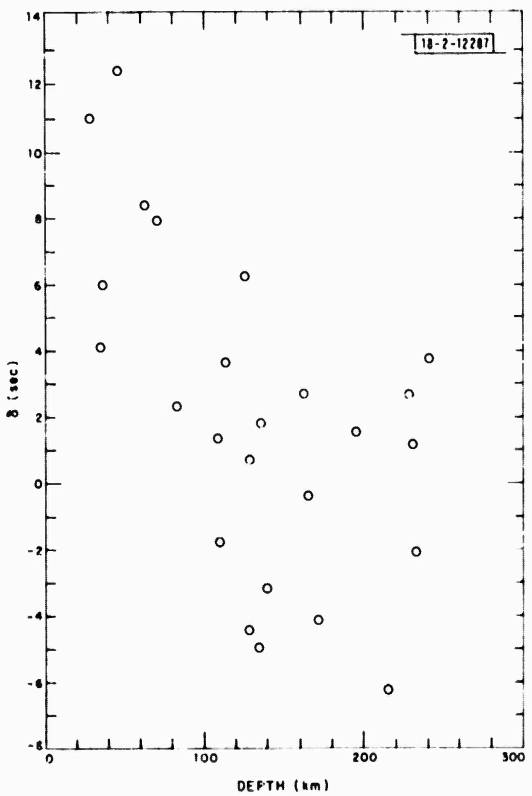

Fig. II-8. Short-period S anomalies at NDI as function of depth from regional earthquakes north of station.

III. NETWORK STUDIES

A. SEISMIC DATA MANAGEMENT SYSTEM

Work is continuing on construction of a management structure for seismic data/information resulting from the Integrated World-Wide Seismic System (IWWSS). The extent and complexity of the IWWSS requires the need of a documentation system capable of handling and sorting much of the detailed information and documents resulting from such a world-wide system. The document-handling utility, NLS, currently in operation at Office-1 on the ARPANET, will serve as the means by which text data and information related to the IWWSS will be sorted, edited, and stored. This facility at Office-1 serves as the utility for text editing, storing, and manipulation of the text files that will ultimately become the foundation for the data management system. Once the basic files are nearly completed, they will then be made available to IWWSS data users and related personnel via the ARPANET and the NLS system.

The acquisition of documents and data related to IWWSS is dependent upon many of the system contractors and development personnel. Once information from them can be obtained, it will be edited and incorporated into the data management system. A close degree of cooperation among users and developers will be necessary to obtain a system of sufficient detail to be of benefit to most users. Several organizations have been contacted and requested to submit information and documentation for inclusion into the system. Documentation that currently exists for IWWSS components which have reached some degree of stability are to be included in the management system. One major problem at present is the large degree of fluidity of many of the current plans for IWWSS. Because of this condition, it is not possible to include many of the major components of IWWSS at this time. Some components that are firmly established, such as datacomputer datalanguage, have already been included into the management system. The document "Datacomputer Version 0/10 User Manual" has been entered in the NLS system and is available for use within NLS. Some restructuring of this manual was necessary to make full use of the capabilities of NLS. The document index, given in the first branch of the file, provides rapid access to any major section of that user manual. Once the user determines the appropriate chapter, section, or topic of interest from the index, the Command "Print Branch" or "Jump (to) Link" will access that area of the document. The index of this file together with those of all other files are contained in a master index file, and will be presented to the user when he enters the NLS system.

Users of the data management system will not necessarily be well versed in NLS command language. To make this information system usable by the entire community, it will be necessary to ask the user (when he enters NLS) if he is familiar with NLS. If he is not acquainted with the NLS language, then he will be presented with a brief introduction to the NLS and IWWSS systems and a subset of NLS commands needed for a "read only" knowledge of the system. Also, in order to make the NLS system seem "cleaner," i.e., less cluttered by heralds, prompts, and echoes, these features are eliminated for the new user. It now appears that a user knowledge of only 8 to 10 commands will be sufficient to acquire a "read only" capability in NLS.

Several files have been set up and now contain the basic information and categories of IWWSS topics. These will be the foundation of the management system, and will be expanded and developed as more information becomes available. In addition to the index file, there is an information file that contains a general description of each file in the management system. Other

Preceding page blank

TABLE III-1

NUMBER OF DETECTING STATIONS

NUMBER OF STATIONS < 90° FROM EVENT	1	2	3	4	5	6	7	8	9	10	11	12	13	14	15	16	17	18	19	20	21	22	23	24	25	26	27	28	29	30	31	32
1	0.630																															
2	0.863	0.197																														
3	0.949	0.691	0.250																													
4	0.981	0.854	0.528	0.158																												
5	0.991	0.933	0.733	0.391	0.099																											
6	0.997	0.971	0.860	0.606	0.283	0.061																										
7	0.999	0.988	0.930	0.766	0.487	0.231	0.039																									
8	1.000	0.995	0.966	0.869	0.663	0.381	0.141	0.025																								
9	1.000	0.998	0.984	0.935	0.793	0.558	0.292	0.098	0.016																							
10	1.000	0.999	0.993	0.964	0.879	0.706	0.460	0.221	0.069	0.010																						
11	1.000	1.000	0.997	0.982	0.933	0.815	0.615	0.371	0.164	0.046	0.006																					
12	1.000	1.000	0.999	0.991	0.964	0.889	0.741	0.525	0.295	0.120	0.031	0.004																				
13	1.000	1.000	0.999	0.996	0.981	0.938	0.835	0.661	0.440	0.230	0.088	0.021	0.002																			
14	1.000	1.000	1.000	0.998	0.991	0.965	0.899	0.770	0.579	0.362	0.177	0.063	0.014	0.002																		
15	1.000	1.000	1.000	0.999	0.995	0.981	0.940	0.851	0.700	0.499	0.294	0.135	0.045	0.010	0.001																	
16	1.000	1.000	1.000	1.000	0.998	0.990	0.968	0.907	0.795	0.625	0.423	0.235	0.102	0.032	0.006	0.001																
17	1.000	1.000	1.000	1.000	0.999	0.995	0.981	0.944	0.866	0.732	0.551	0.353	0.186	0.076	0.022	0.004	0.000															
18	1.000	1.000	1.000	1.000	0.999	0.997	0.990	0.967	0.915	0.816	0.665	0.478	0.291	0.145	0.056	0.016	0.003	0.000														
19	1.000	1.000	1.000	1.000	1.000	0.999	0.995	0.981	0.948	0.879	0.760	0.596	0.409	0.237	0.112	0.041	0.011	0.002	0.000													
20	1.000	1.000	1.000	1.000	1.000	0.999	0.997	0.990	0.969	0.922	0.835	0.699	0.527	0.345	0.191	0.086	0.030	0.008	0.001	0.000												
21	1.000	1.000	1.000	1.000	1.000	1.000	0.999	0.994	0.982	0.952	0.890	0.785	0.635	0.459	0.280	0.152	0.065	0.022	0.005	0.001	0.000											
22	1.000	1.000	1.000	1.000	1.000	1.000	0.999	0.997	0.990	0.971	0.929	0.851	0.730	0.570	0.396	0.238	0.120	0.049	0.016	0.004	0.001	0.000										
23	1.000	1.000	1.000	1.000	1.000	1.000	1.000	0.998	0.994	0.983	0.955	0.900	0.806	0.671	0.506	0.338	0.194	0.094	0.037	0.011	0.002	0.000	0.000									
24	1.000	1.000	1.000	1.000	1.000	1.000	1.000	0.999	0.997	0.990	0.973	0.935	0.865	0.756	0.610	0.444	0.285	0.157	0.073	0.027	0.008	0.002	0.000	0.000								
25	1.000	1.000	1.000	1.000	1.000	1.000	1.000	1.000	0.998	0.994	0.984	0.959	0.909	0.825	0.702	0.548	0.385	0.237	0.126	0.056	0.020	0.006	0.001	0.000	0.000							
26	1.000	1.000	1.000	1.000	1.000	1.000	1.000	1.000	0.999	0.997	0.990	0.974	0.940	0.874	0.779	0.645	0.488	0.330	0.196	0.100	0.043	0.015	0.004	0.001	0.000	0.000						
27	1.000	1.000	1.000	1.000	1.000	1.000	1.000	1.000	0.999	0.998	0.994	0.984	0.962	0.917	0.842	0.730	0.587	0.429	0.281	0.161	0.079	0.032	0.011	0.003	0.001	0.000	0.000					
28	1.000	1.000	1.000	1.000	1.000	1.000	1.000	1.000	1.000	0.999	0.997	0.991	0.976	0.945	0.889	0.800	0.677	0.529	0.374	0.236	0.130	0.062	0.024	0.008	0.002	0.000	0.000	0.000				
29	1.000	1.000	1.000	1.000	1.000	1.000	1.000	1.000	1.000	0.999	0.998	0.995	0.985	0.965	0.925	0.856	0.754	0.622	0.472	0.323	0.197	0.105	0.048	0.018	0.006	0.001	0.000	0.000	0.000			
30	1.000	1.000	1.000	1.000	1.000	1.000	1.000	1.000	1.000	1.000	0.999	0.997	0.991	0.978	0.950	0.899	0.819	0.705	0.566	0.417	0.277	0.163	0.084	0.037	0.014	0.004	0.001	0.000	0.000	0.000		
31	1.000	1.000	1.000	1.000	1.000	1.000	1.000	1.000	1.000	1.000	0.999	0.998	0.995	0.986	0.967	0.931	0.868	0.777	0.654	0.511	0.365	0.234	0.134	0.066	0.028	0.010	0.003	0.001	0.000	0.000	0.000	
32	1.000	1.000	1.000	1.000	1.000	1.000	1.000	1.000	1.000	1.000	1.000	0.999	0.997	0.992	0.979	0.954	0.908	0.835	0.731	0.601	0.457	0.317	0.197	0.109	0.052	0.022	0.007	0.002	0.000	0.000	0.000	0.000

Single-station probability = 0.63.

currently available files include one with the personnel names, organizations, and organizational responsibilities for the IWWSS. One other file is dedicated to a description of all SROs and all other seismic sites that make up part of the IWWSS. A complete site description and location will be provided along with descriptions of the instrumentation at each site as soon as these sites become operational.

R. M. Sheppard

B. DETECTION CAPABILITY OF A 32-STATION SUBSET OF ISM STATIONS DURING THE ISM PERIOD

An investigation into the detection capability of a 32-station subset (Fig. III-1) of the approximately 150 stations used by the ISM experiment[1] has been completed. A simple statistical model to predict the probability of an N-station detection from an M-station network was developed. The data from the 32-station set were used to estimate the single-station detection probability for events with $4.6 \leq m_b < 4.7$ and within 90° of the station. This probability was entered into the model, and a network detection probability table was generated. A Technical Note reporting the detailed results of this investigation is in preparation.

The selection of the 32-station subset was ad hoc to give good global coverage while using stations which contributed data to a large number of ISM events. The ISM event list is composed of 996 events which occurred between 20 February and 19 March 1972. The subset stations detected and located 819 of these events. Many of the 177 events, reported on the ISM list but not reported on the subset list, were small events requiring a more compact geographically distributed network than the subset network, to meet the epicenter location criteria used by this experiment.

A comparison was made between the USGS PDE list and the event list created using the 32-station subset network. The subset list showed 508 events not reported by the PDE list, while the PDE list reported 43 events not included in the subset list. All the stations used in the computation of events listed by the subset network, with the exception of CHG and YKA, were contributers to the PDE computations. However, the detection and reporting level to USGS and for our experiment were quite different. For example, the detection and reporting level for the USGS and for the ISM subset were compared for stations MBC and KBL. The additional detections available to Lincoln vastly improved the stations' detection capability for events with $m_b < 4.5$.

Using the 32-station subset network of well read and reported stations, a single-station detection probability of 0.63 was estimated for events with $4.6 \leq m_b < 4.7$ and $\Delta \leq 90°$. Table III-1 shows how this converts into network detection probability. For example, if 20 stations of the subset are within 90° of an event m_b of 4.6, the probability is 100 percent that 5 of these stations will detect it and the probability is greater than 90 percent that 10 stations of the subset will detect it.

R. E. Needham

C. SEISMIC EVENT LOCATION PROCEDURES

The event-location program developed for the ISM project[2] is undergoing continuing modification and improvement. These changes include: (1) the addition of new seismic phases, (2) the ability to restrain latitude and/or longitude and/or origin time, as well as focal depth, and (3) provision for attempting to automatically identify and reject observations inconsistent with the other data. This last provision is particularly useful because data are frequently contaminated by a few gross errors, the detection of which consumes a great deal of analysts' time. Tables III-2(a) and (b) show an example from the ISM: an earthquake in the southern Kuril Islands.

TABLE III-2(a)
INITIAL (ISM) LOCATION

LAT: 43.940 LONI 148.17* DEPTH: 29.0 KM ORIGIN TIME: 201 H 29.1 SEC

STA	DELTA (DEG)	AZIMUTH EP (DEG)	AZIMUTH STA (DEG)	PHASE		TIME (SEC)	RESID (SEC)	SIGMA (SEC)	DT/DD (SEC/DEG)	AZ (DEG)	RESIDUAL MAG (S/DEG)	RESIDUAL DIR (DEG)	RESIDUAL SIGMA (S/DEG)	WT
MAT	10.604	229.2	42.8	1	P	149.9	-1.8	3.0						0.98
COL	48.508	36.2	278.8	1	P	457.9	0.3	1.5						0.98
GIL	48.634	36.1	271.2	1	P	457.9	-0.7	1.5						0.98
INK	45.877	38.5	279.8	1	P	500.9	0.3	1.5						0.98
CHG	48.039	254.7	47.3	1	P	517.9	0.4	1.5						0.98
RES	54.574	16.9	307.8	1	P	575.9	-0.4	1.5						0.98
YKA	55.234	34.1	299.3	1	P	578.9	-0.1	1.5						0.98
YKA	55.234	34.1	299.3	1	S				7.32	302.0	0.36	13.0	0.80	0.98
KBL	59.817	298.3	55.2	1	P	623.9	0.6	1.5						0.98
BMO	63.547	52.4	306.5	1	P	628.9	0.5	1.5						0.98
NUR	66.282	333.3	41.2	1	P	646.9	1.3	1.5						0.98
EUR	67.418	56.4	300.2	1	P	654.9	0.2	1.5						0.96
LAO	68.424	45.5	311.6	1	P				6.32	311.4	0.32	-165.2	0.40	0.98
LAO	68.424	45.5	311.6	1	P	658.9	-0.9	1.5						0.98
FRC	68.819	16.5	332.5	1	P	661.9	-0.4	1.5						0.98
OUG	69.035	54.1	310.2	1	P	662.9	-0.7	1.5						0.98
UPP	69.902	335.7	34.2	1	P	663.9	1.1	1.5						0.98
NAO	69.973	339.3	31.4	1	P				6.25	36.7	0.58	122.0	0.40	0.98
NAO	69.973	339.3	31.4	1	P	667.9	-1.6	1.5						0.98
HFS	69.798	337.4	33.3	1	P	668.9	0.5	1.5						0.98
LAO	68.424	45.5	311.6	1	S	670.9	2.5	1.5						0.98
URO	70.829	52.3	311.4	1	P	674.9	0.1	1.5						0.98
NAO	69.973	339.3	31.4	1	S	675.9	-2.3	1.5						0.98
CLL	77.483	333.2	31.4	1	P	713.9	-0.1	1.5						0.96
PRA	78.057	331.4	32.2	1	P	718.9	1.7	1.5						0.98
MOX	78.504	333.5	32.5	1	P	719.9	0.1	1.5						0.98
GRF	79.458	333.2	32.1	1	P	725.9	0.8	1.5						0.98
SSC	83.743	339.4	22.5	1	P	746.9	-0.9	1.5						0.98
GRR	84.113	339.8	21.9	1	P	749.9	0.2	1.5						0.98

CHI SQUARED = 13.32 ON 28 DEGREES OF FREEDOM.

TABLE III-2(b)

FINAL LOCATION

LAT: 43.779 LON: 148.32? DEPTH: 38.7 KM ORIGIN TIME: 201 M 28.8 SEC

STA	DELTA (DEG)	AZIMUTH FR (DEG)	AZIMUTH STA (DEG)	PHASE		TIME (SEC)	RESID (SEC)	SIGMA (SEC)	DT/DD (SEC/DEG)	AZ (DEG)	RESIDUAL MAG (S/DEG)	RESIDUAL DIR (DEG)	RESIDUAL SIGMA (S/DEG)	WT
MAT	10,583	230,?	43,9	1	?	149,2	-1,8	3,0						0,96
COL	40,574	36,1	220,5	1	?	457,2	0,2	1,5						0,98
GIL	42,780	36,?	220,7	1	?	457,2	-0,8	1,5						0,96
INK	45,961	3?,4	229,5	1	?	500,2	0,?	1,5						0,98
CHG	48,101	254,9	47,8	1	?	517,2	0,?	1,5						0,98
RES	54,696	14,9	307,8	1	?	565,2	-0,8	1,5						0,97
YKA	55,30?	34,?	299,?	1	?	570,2	-0,?	1,5						0,98
YKA	5?,306	34,1	299,?	1	?				7,32	302,0	0,39	13,2	0,80	0,97
KBL	59,975	29?,?	55,?	1	?	603,2	-0,?	1,5						0,98
BMO	63,559	52,4	304,?	1	?	628,2	1,?	1,5						0,95
NUR	64,395	333,?	41,1	1	?	646,2	0,6	1,5						0,97
EUR	67,614	56,4	309,8	1	?	654,2	0,7	1,5						0,97
LAO	68,459	45,?	311,4	1	?				6,32	311,4	0,01	86,6	0,40	0,98
LAO	68,459	45,?	311,4	1	?	658,2	-0,6	1,5						0,97
FBC	68,942	14,6	332,3	1	?	661,2	-0,7	1,5						0,97
DUG	69,042	54,1	310,?	1	?	662,2	-0,3	1,5						0,98
UPP	69,093	335,?	36,?	1	?	663,2	0,4	1,5						0,98
NAO	70,162	339,4	31,4	1	?				6,25	36,7	0,58	120,0	0,40	0,44
NAO	70,162	339,4	31,4	1	?	667,2	-2,3	1,5						0,33
HFS	69,988	337,7	33,3	1	?	668,2	-0,?	1,5						0,98
LAO	68,459	45,?	311,4	1	1	670,2	0,4	1,5						0,96
UBO	70,843	52,?	311,4	1	?	674,2	0,5	1,5						0,98
NAO	70,162	339,4	31,4	1	1	675,2	-5,3	1,5						0,00
CLL	77,676	338,1	31,4	1	?	713,2	-0,7	1,5						0,97
PRA	78,258	331,7	32,2	1	?	718,2	1,1	1,5						0,95
MOX	78,696	333,4	30,4	1	?	719,2	-0,4	1,5						0,98
GRF	79,651	333,?	30,1	1	?	725,2	0,3	1,5						0,98
SSC	83,932	339,?	29,4	1	?	746,2	-1,3	1,5						0,91
GRR	84,302	339,9	21,9	1	?	749,2	-0,2	1,5						0,98

CHI SQUARED = ?,96 ON 28 DEGREES OF FREEDOM,

Although there is nothing obviously wrong with the epicenter determined for the ISM, a much better fit to the data (and an 18-km shift of the epicenter) is obtained if the arrival time data from NORSAR are discarded.

A Technical Note describing the location program in detail is in preparation.

B. R. Julian

D. STABILITY OF TELESEISMIC TRAVEL-TIME RESIDUALS

It has been shown that seismic wave velocities in seismic regions may change with time, and one way of measuring this variation, particularly when a dense local network is unavailable, is to study teleseismic P-wave travel-time residuals at a particular station to see whether these are subject to temporal variation.[3,4] Such changes in travel time will obviously have a measurable effect on the location ability of a seismic network. Considerable care must be exercised to ensure that the variations observed (~0.2 to 0.4 sec) do not arise from epicenter migration, location errors, station timing errors, and many other factors, and in general only deep events are used and the residual averaged over intervals of about 6 months. A suitable way to test the stability, or lack of it, of residuals is to study those determined at teleseismic distances for nuclear explosions at the Nevada Test Site (NTS). Here the location, origin time, and depth are known for over 100 useful events over the last 10 years, and the only errors left are those in station timing and reading and possibly from movement of shot location within NTS.

For 20 stations which have regularly reported arrivals from NTS events over 1964 to 1972, the travel-time residuals calculated by the International Seismological Center (ISC) with respect to the locations given by the AEC were plotted as a function of time. An immediately noticeable feature of the results was a variation from station-to-station of the spread and standard deviation of the residuals. This could be due to reading or timing errors, grossly heterogeneous substation structure, or to "kinks" in the travel-time curve. Stations giving consistent residuals with a standard error of less than 0.3 sec included UME, SOD, ARE, GIL, NPR, and KTG. Standard errors in excess of 0.5 sec were observed for TRO, KON, GRR, FLN, SSF, and COL (Fig. III-2).

Larger residuals (earlier arrivals) were almost invariably observed for the larger shots, either because of better time picks or the greater shot depths used. Shot elevations (above sea level) range from 0.5 to 1.9 km, introducing a non-negligible travel-time correction which was not included by the ISC. By assuming a near-surface velocity of 2.5 km/sec to correct for depth, these times could be moved closer to the mean. A study of the correlation of location within NTS with residual values yielded negative results.

At two stations, ADK (Adak) and MAT (Matsushiro), apparent temporal variations in residual values were observed both of ~0.5-sec magnitude and durations 2 to 3 years. These are shown in Fig. III-3, the variation in both cases commencing in late 1967. A comparison of residuals at pairs of close stations, such as (GRR-FLN), (FLN-LOR) (France) reveals that the standard error of the difference in residual between them is significantly less than the error in that for the individual stations. This indicates that heterogeneity near some stations may be the cause of the large standard errors observed. In some instances, e.g., COL, this is obviously not the case, since at a very close station (GIL) the standard deviation of the residual was only 0.24 sec compared with 0.54 sec for the former. This can only be ascribed to bad time picks, and emphasizes that considerable caution must be exercised in using bulletin data.

R. G. North

REFERENCES

1. R.T. Lacoss, R.E. Needham and B.R. Julian, "International Seismic Month Event List," Technical Note 1974-14, Lincoln Laboratory, M.I.T. (27 February 1974), DDC AD-776021/8.
2. Seismic Discrimination SATS, Lincoln Laboratory, M.I.T. (30 June 1973), DDC AD-766559/9.
3. M. Wyss and D.J. Holcomb, "Earthquake Prediction Based on Station Residuals," Nature 245, 139 (1973).
4. M. Wyss and A.C. Johnston, "A Search for Teleseismic P Residual Changes Before Large Earthquakes in New Zealand," J. Geophys. Res. 79, 3283 (1974).

Fig. III-1. Locations of stations used in 32-station network.

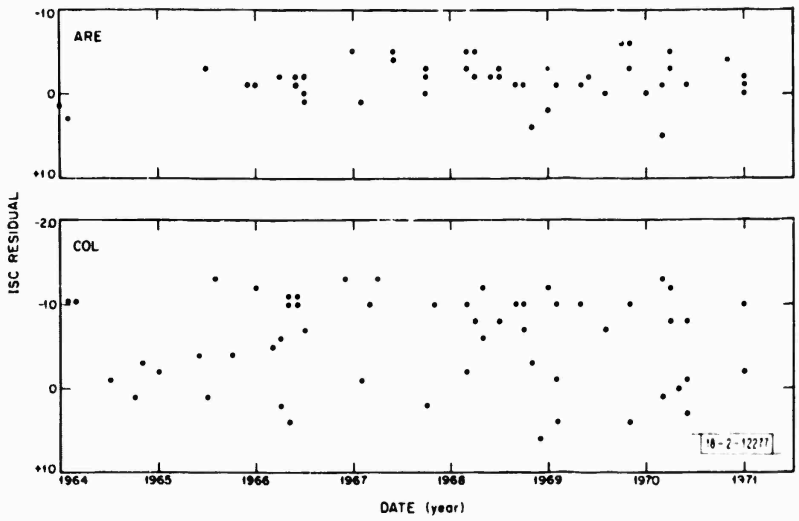

Fig. III-2. P-wave travel-time residuals from NTS at ARE (Arequipa, Peru, Δ = 67.8°) and COL (College, Alaska, Δ = 33.5°). ARE readings appear, with standard deviation of 0.25 sec, to be much better than those at COL (σ = 0.54).

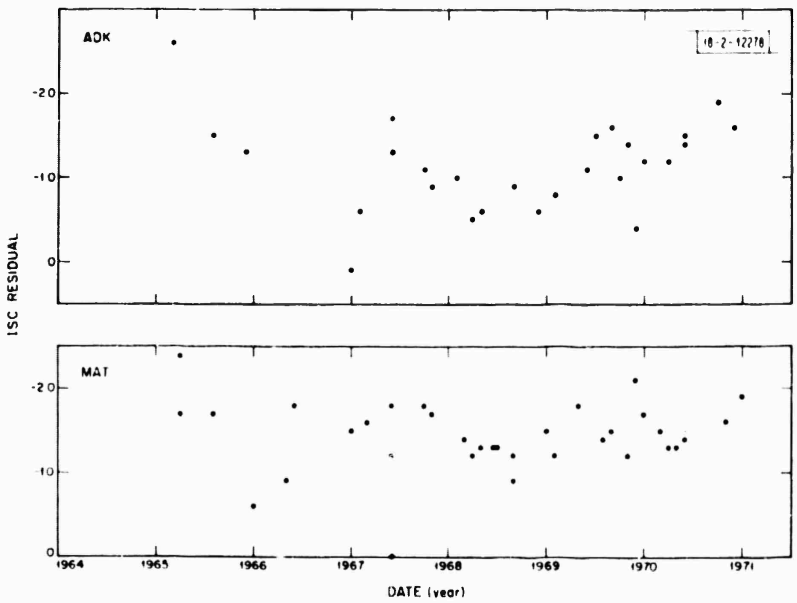

Fig. III-3. Apparent time variation of residuals from NTS at ADK (Adak, Aleutians, Δ = 44.4°) and MAT (Matsushiro, Japan, Δ = 79.6°). In both cases, residual appears to deviate by about 0.5 sec from mean for 2-year period commencing in mid-1967.

IV. EARTH HETEROGENEITY

A. EVIDENCE FOR ANISOTROPIC SCATTERING IN THE UPPER MANTLE, DEDUCED FROM P, pP, PcP, AND pPcP PHASES

In a previous study[1] of the core mantle boundary, we observed that short-period PcP/P amplitude ratios measured at LASA are a strong function of focus depth. Shallow events from 0- to 100-km depth have PcP/P ratios 3 to 4 times the ratios for events deeper than 200 km. Our conclusion was that a strong scattering mechanism in the upper mantle rather than inelastic attenuation was producing the observed depth effect of PcP/P ratio. This scattering is not isotropic but is a strong function of the horizontal phase velocity of the rays passing through the upper mantle. Rays of high $dT/d\Delta$ are attenuated more than waves of low $dT/d\Delta$ along comparable path lengths.

Additional data have been obtained which clearly isolate the scattering effect to the upper mantle above the focus. This is done by using the surface-reflected phases pP and pPcP in conjunction with P and PcP phases. Figure IV-1 shows the ray paths for these phases for a particular distance and focus depth. In order to isolate the upper-mantle ray paths, we computed the ratio of pPcP/pP to PcP/P amplitudes for 20 LASA events. There are several advantages to using this ratio:

(1) The takeoff angles of pPcP and pP are very close at teleseismic distances, and one may assume that similar source amplitudes are radiated along each direction. Similarly, one can assume equal source radiation along the ray paths of PcP- and P-waves. By taking (pPcP/pP)/(PcP/P) ratios, we thus eliminate the unequal source radiation in the up-and-down directions from the focus.

(2) Reflection coefficients at the free surface divide out because the incident angles of pPcP and pP are nearly equal.

(3) pPcP and PcP rays sample the same part of the core mantle boundary and experience the same spherical spreading as a function of distance and depth. Also, pP and P sample the same part of the lower mantle. Thus, the ratio (pPcP/pP)/(PcP/P) cancels the spherical spreading, attenuation, and core mantle boundary reflection. This essentially eliminates the earth structure below the source and isolates the effects of the mantle above the source.

Figure IV-2 shows the (pPcP/pP)/(PcP/P) amplitude ratios for 20 events recorded at LASA as a function of epicentral distance. The amplitude ratios vary by almost an order of magnitude with no trend with distance. The same data are plotted as a function of focus depth in Fig. IV-3. Except for one data point, there is a clear trend of this ratio from 1 for the shallowest event, to 3 or greater at depths >200 km. The values are scattered but significantly >1 in all cases except one. As previously discussed, these amplitude ratios should cancel out the earth model effects below the source, and isolate the ray paths above the source.

Figure IV-4 shows the theoretical effect of Kanamori's Q model[2] on (pPcP/pP)/(PcP/P) ratios as a function of depth, distance, and peak frequency of the phases. At 1 Hz, the effect of attenuation is to elevate the ratio smoothly with depth to values >1. This effect increases with depth of focus, depending on the epicentral distance as shown by the solid lines for 40° and 80°. At 0 Hz, no attenuation would occur and the region would collapse into a single line of value 1 for all depths and distances.

The effect of attenuation was removed from the data using Kanamori's Q model. The corrected (pPcP/pP)/(pP/P) ratios are shown in Fig. IV-5. If the uncorrected ratios were explained by such a low Q model, then the corrected ratios in this figure would scatter about 1.0 for all depths. However, the corrected ratios are still significantly above 1. In order to correct the ratios to a level of ~1 for all depths, an average Q of <40 for the upper 400 km of the mantle would be required.

Such low Q values for short-period data are clearly unacceptable. One explanation is an anisotropic scattering mechanism, which attenuates the ray paths above the source for pP phases more severely than pPcP phases. As previously suggested,[1] thin horizontal laminations of low rigidity sandwiched between thick layers of solid material could produce such a phenomenon. Theoretical studies of scattering of P-waves through more realistic mantle models are being undertaken.

C. W. Frasier
D. K. Chowdhury

B. SCATTERING OF ELASTIC WAVES IN A MEDIUM WITH ANISOTROPICALLY DISTRIBUTED RANDOM INHOMOGENEITIES

Previous theoretical studies of elastic wave scattering[3-5] in random media have dealt only with the case in which the inhomogeneities are distributed without regard to spatial orientation. However, recent studies of PcP/P amplitude ratios[1,6] suggest that in the upper mantle, P-wave scattering depends strongly on the angle of incidence, an effect which cannot be explained by these isotropic theories. The results of these studies also indicate that a significant fraction of the energy (50 percent or more) in short-period P-waves may be scattered in a single passage through the upper mantle, a phenomenon potentially capable of seriously biasing many types of seismic investigations.

We have extended the theory given by Knopoff and Hudson[4,5] to the case of a medium with an anisotropic distribution of random inhomogeneities. That is, the elastic constants λ and μ and the density ρ are assumed to be functions of position r given by

$$\lambda = \lambda_o + \delta\lambda(\bar{r}) \quad ; \quad \mu = \mu_o + \delta\mu(\bar{r}) \quad ; \quad \rho = \rho_o + \delta\rho(\bar{r})$$

where $\delta\lambda$, $\delta\mu$, and $\delta\rho$ are specified only in terms of their correlation function:

$$N\lambda(\bar{r}_1, \bar{r}_2) = \langle \delta\lambda(\bar{r}_1),\ \delta\lambda(\bar{r}_2) \rangle \qquad N\lambda\mu(\bar{r}_1, \bar{r}_2) = \langle \delta\lambda(\bar{r}_1),\ \delta\mu(\bar{r}_2) \rangle$$

$$N\mu(\bar{r}_1, \bar{r}_2) = \langle \delta\mu(\bar{r}_1),\ \delta\mu(\bar{r}_2) \rangle \qquad N\mu\rho(\bar{r}_1, \bar{r}_2) = \langle \delta\mu(\bar{r}_1),\ \delta\rho(\bar{r}_2) \rangle$$

$$N\rho(\bar{r}_1, \bar{r}_2) = \langle \delta\rho(\bar{r}_1),\ \delta\rho(\bar{r}_2) \rangle \qquad N\lambda\rho(\bar{r}_1, \bar{r}_2) = \langle \delta\lambda(\bar{r}_1),\ \delta\rho(\bar{r}_2) \rangle$$

where the brackets $\langle\ \rangle$ indicate averaging over the ensemble of all possible inhomogeneities. Previous studies such as Knopoff and Hudson[4,5] have assumed these correlations to be functions of $|\bar{r}_1 - \bar{r}_2|$, usually of Gaussian form:

$$N(\bar{r}_1, \bar{r}_2) = \sigma^2 \exp\left[-\frac{|\bar{r}_1 - \bar{r}_2|^2}{a^2} \right]$$

whereas we have used

$$N(\bar{r}_1, \bar{r}_2) = \sigma^2 \exp\left[-\frac{(x_1 - x_2)^2}{a^2} - \frac{(y_1 - y_2)^2}{b^2} - \frac{(z_1 - z_2)^2}{c^2} \right] .$$

Figure IV-6 gives some preliminary results for P-to-P scattering, comparing the isotropic case with the case in which a = b = 5c. It is evident from these results that anisotropy in the distribution of inhomogeneities profoundly effects the scattering of elastic waves, and in fact that the most energy is scattered in a direction controlled by the "grain" of the medium, rather than by the direction of the incident wave.

A paper containing more details of the theory and compiling results for a variety of cases (including P-to-S, S-to-P, and S-to-S scattering) is in preparation.

W. B. Lee
B. R. Julian

C. SCATTERING IN THE MID-TO-UPPER MANTLE

Both forward and backward scattering by random inhomogeneities within the crust have been suggested as sources of short-period seismic codas.[6,7] Forward scattering at or near the core-mantle boundary has been invoked as a source of precursors to PKKP and PKP.[8,9] Here a simple model for teleseismic scattering is suggested, and evidence is presented that strong scattering occurs in the mid-to-upper mantle.

Since multiple scattering greatly reduces the scattered energy in a given direction, a model is assumed in which singly scattered waves contain the major scattering energy. To isolate scattered energy from mantle regions, short-period codas between major phases from shadow zone events have been analyzed. This technique greatly reduces the complexity of the seismograms to be studied. Figure IV-7 represents a cross section of the earth showing the shadow zones for two events that are more than 95° apart, at points A and B. The ray AP_A is the P-wave path that grazes the core and defines the strictly geometrical core shadow. The ray AP_A^d defines the last observable ray path of P diffracted in the geometrical shadow zone for a source at A and a receiver at P_A^d. BP_B and BP_B^d represent the same paths for a source at point B.

Assuming a receiver at point A is used to study an event from point B, it is evident that only inhomogeneities that lie within the intersection of the regions above the two true shadow zones can contribute singly scattered signals. The arrival time of scattered waves at point A for each scattering point (e.g., points 1 and 2 in Fig. IV-7) may be calculated as the sum of the wavefront times which intersect at that point. This arrival time plus the observed slowness at A define the location of the scatterer. For example, scattering at points 1 and 2 would result in scattered travel times of 17 minutes for the configuration of source and receiver shown, but waves from these two points would arrive at point A with quite different slownesses.

Of course, the model is not restricted to only P-to-P scattering; P-to-S and S-to-P scattering might also occur. Referring to points 1 and 2 again, and assuming a v_p/v_s ratio of 2, the travel time to point A of the scattered waves would be 27 minutes.

Figure IV-8 shows a possible application of this model to results obtained from the study of the two following shallow events near the Philippine Islands:

Δ	Azimuth
105°	305°
107°	303°

Short-period data from the LASA E- and F-rings were bandpass filtered with a window of 0.9 ± 0.4 Hz. These data were then used to form Vespagrams. In both cases, an arrival was found at 17 minutes ± 4 sec after the event time with a slowness of 6.4 sec-deg^{-1}. This slowness corresponds to a P-wave arrival from a distance of 64°. The intersection of this ray with the 17-minute isotime line defines the position of the proposed scatterer. This places the scatterer at a depth of about 1000 km under the intersection of the American and Pacific plates and the great circle path. Analysis of a third event from the same region but at a greater distance (121°) also provided an arrival appropriate to this scatterer. Of course, the energy in this arrival could be equally well due to multiple scattering in the receiver region of a late P-phase. This will be resolved by undertaking frequency-wavenumber spectral analysis of these events.

J. Scheimer
A. V. Nikolaev
T. E. Landers

D. SHEAR WAVE VELOCITY IN THE EARTH'S LOWER MANTLE

Unlike compressional velocity, the shear velocity in the earth's mantle is known so far at best within an uncertainty of 0.1 km/sec or more. Recent observations of large numbers of overtones of normal modes have given us, however, a better estimate of shear velocity (see, for example, Gilbert and Dziewonski[10]). Precise estimates for radial variation in shear velocity have become important now more than ever as present knowledge of the earth is getting more complex radially and laterally. Any kind of thermally activated inhomogeneity would affect shear velocity more than compressional velocity, and thus shear velocity variation would be a sensitive indicator for the presence of thermal plumes or mantle-wide thermal convection. At the present time, body wave travel time and amplitude data are more effective tools for studying lateral heterogeneity in the earth's mantle than the normal mode data. Therefore, we need a body wave standard for shear velocity, eliminating any possibility of inconsistency among normal mode data and body wave data due to difference in the wavelength involved.

A standard for radial variation in shear velocity has been obtained from the inversion of deep shock travel-time data, thus eliminating the effect of near-source heterogeneity in the upper mantle and enhancing the reading accuracy. Our velocity model is presented in Fig. IV-9 and is tabulated in Table IV-1. Nonuniqueness in this velocity model has been studied in the framework of the inversion theory of Backus and Gilbert.[11] According to this theory, the vertical error bar (Fig. IV-9) in our velocity model (termed "spread") results from the finiteness in the number of the observed data and gives a measure of resolving length. The horizontal bar (Fig. IV-9), on the other hand, arises due to error in the observation and also due to the inadequacy of the model in fitting the observed data. These two errors – spread and error in velocity – are not independent but one can be reduced at the expense of the other. The functional relationship between the two errors, commonly known as "trade-off curves," is shown in Fig. IV-10 for different depths in the lower mantle. One immediate application of these trade-off curves is to assert that, with our data, one cannot parameterize the shear velocity model with 50-km-thick and resolvable layers in the mantle. Such a parameterization would lead to an error in the computed travel times of a larger magnitude than observed. The resolving kernels for corresponding depths are shown in Fig. IV-11. These resolving kernels show that error in the assumed shear velocity distribution in the upper mantle would not affect the velocity model in the lower mantle below 1000 km. Apart

TABLE IV-1

S MODEL: MKS1S-A

Depth (km)	Velocity (km/sec)	Spread/2.0 (km)	Standard Error (km/sec)
671	6.111	195	0.071
721	6.153	163	0.049
771	6.184	141	0.050
821	6.213	144	0.048
871	6.232	127	0.040
946	6.281	133	0.033
1021	6.366	125	0.026
1096	6.458	80	0.023
1171	6.490	65	0.021
1246	6.531	87	0.018
1321	6.584	68	0.018
1396	6.604	64	0.020
1471	6.634	58	0.016
1546	6.668	86	0.016
1621	6.727	65	0.016
1696	6.764	55	0.018
1771	6.788	68	0.016
1846	6.821	65	0.016
1921	6.864	75	0.014
1996	6.898	62	0.014
2071	6.938	59	0.015
2146	6.982	50	0.015
2221	7.011	46	0.016
2296	7.043	48	0.017
2371	7.061	56	0.019
2446	7.079	72	0.011
2521	7.115	73	0.012
2596	7.148	68	0.015
2671	7.177	61	0.015
2746	7.199	75	0.015
2821	7.229	54	0.018
2361	7.236	45	0.023
2886	7.247	73	0.049

from the reliable estimates of velocity, other features of our shear velocity model include the absence of velocity inversion near the core mantle boundary, and fluctuations of long wavelength throughout the mantle. Among all the existing shear velocity models, our model comes closest to the 1066 B model of Gilbert and Dziewonski[10] which was obtained from 1064 normal mode fundamental and overtone eigenperiods.

M. K. Sengupta
B. R. Julian

REFERENCES

1. C. W. Frasier and D. K. Chowdhury, "Effect of Scattering on PcP/P Amplitude Ratios at Lasa from 40° to 84° Distance" J. Geophys. Res. 79, 5469-5477 (1974).
2. H. Kanamori, "Spectrum of P and PcP in Relation to the Mantle-Core Boundary and Attenuation in the Mantle," J. Geophys. Res. 72, 559-571 (1967).
3. L. A. Chernov, Wave Propagation in a Random Medium (McGraw-Hill, New York, 1960).
4. L. Knopoff and J. A. Hudson, "Scattering of Elastic Waves by Small Inhomogeneities," J. Acoust. Soc. Am. 36, 338-343 (1964).
5. L. Knopoff and J. A. Hudson, "Frequency Dependence of Amplitude of Scattered Waves," J. Acoust. Soc. Am. 43, 18-20 (1967).
6. Seismic Discrimination SATS Lincoln Laboratory, M.I.T. (30 June 1974), DDC AD-785377/3.
7. K. Aki and B. Chouet, "Origin of Coda Waves; Source, Attenuation, and Scattering Effects" (in press, 1974).
8. D. J. Doornbos, "Seismic Wave Scattering Near Caustics: Observations of PKKP Precursors," Nature 247, 352-353 (1974).
9. R. A. W. Haddon, "Corrugations on the Mantle-Core Boundary or Transition Layers Between Inner and Outer Cores?" (Abstract), Trans. Am. Geophys. Union 53, 600 (1972).
10. F. Gilbert and A. M. Dziewonski, "An Application of Normal Mode Theory to the Retrieval of Structural Parameters and Source Mechanisms for Seismic Spectra" (in press, 1974).
11. G. Backus and F. Gilbert, "Uniqueness in the Inversion of Inaccurate Gross Earth Data," Phil. Trans. Roy. Soc. London 266A, 123-192 (1970).

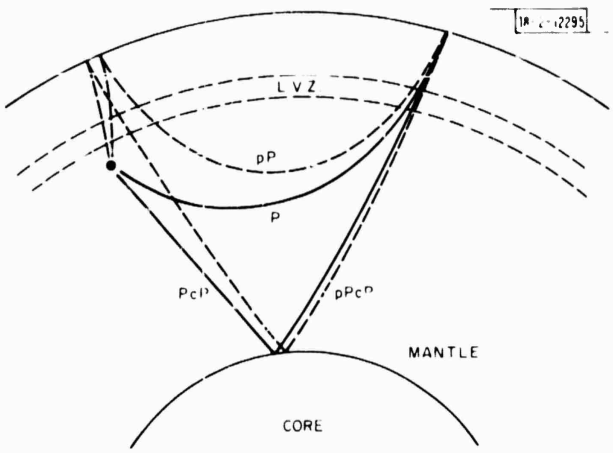

Fig. IV-1. Ray paths for P, pP, PcP, and pPcP phases recorded at same epicentral distance. L.V.Z. denotes low velocity zone of upper mantle.

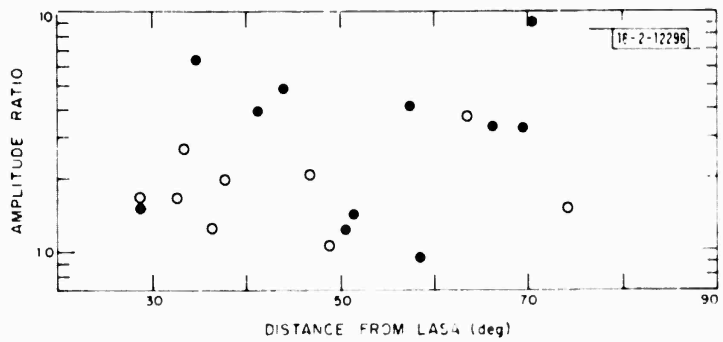

Fig. IV-2. Amplitude ratios (pPcP/pP)/(PcP/P) for 20 events recorded at LASA. Open circles denote earthquakes south of LASA, whereas black circles are events from north.

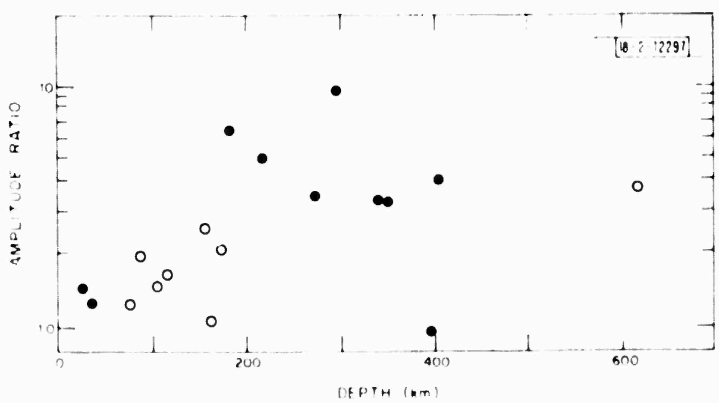

Fig. IV-3. Amplitude ratios (pPcP/pP)/(PcP/P) for 20 events as a function of focus depth.

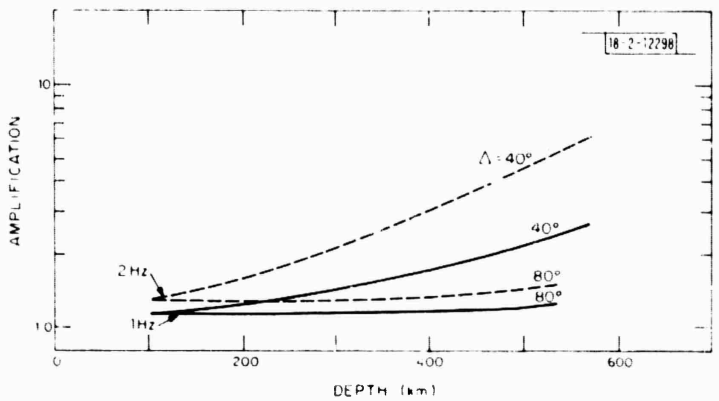

Fig. IV-4. Effect of attenuation on (pPcP/pP)/(PcP/P) ratios as a function of distance, depth of focus, and frequency. Kanamori's Q model (1967) is used.

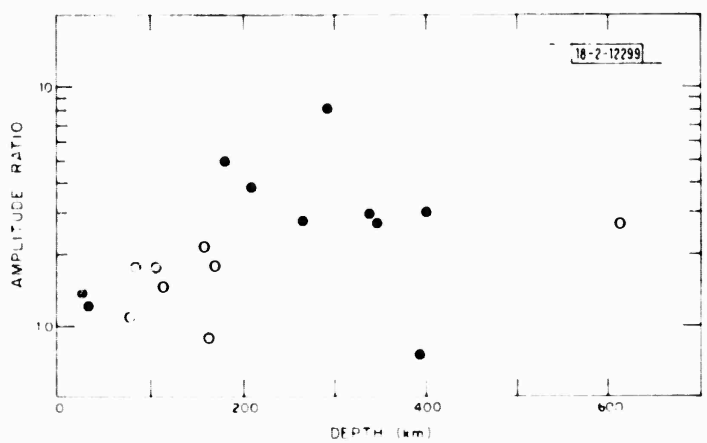

Fig. IV-5. Amplitude ratios (pPcP/pP)/(PcP/P) of Fig. IV-2 corrected for Kanamori's Q model.

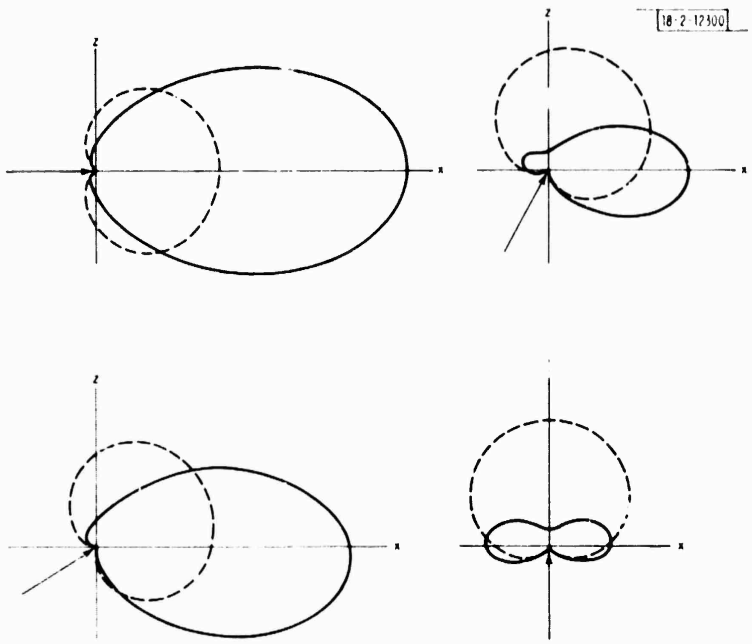

Fig. IV-6. Directional dependence of amplitude of P-waves scattered from incident P-wave in case where correlation lengths are 5 times greater in horizontal (x and y) directions than in vertical (z) direction. Arrows indicate directions of incident waves (0°, 30°, 60°, and 90° to +x axis). For comparison, dashed line gives corresponding result for isotropic case.

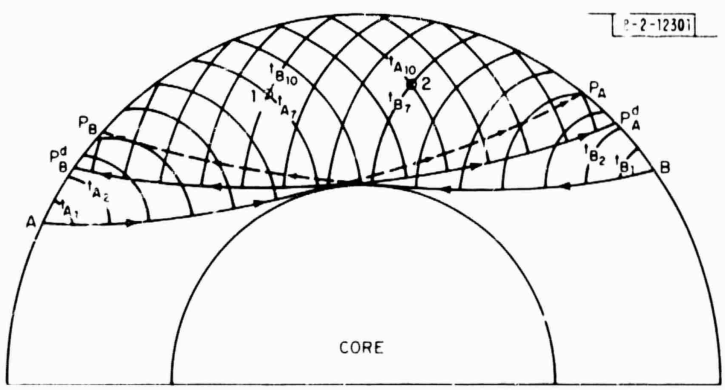

Fig. IV-7. Shadow zones for two events >95° apart. Rays P_A and P_B define strictly geometrical shadow zones for events at points A and B. Rays P_A^d and P_B^d are typical paths for diffracted P-waves from these sources. Arcs represent position of P-wave wavefront from each source at successive 1-minute intervals. Thus, t_{A_1}, t_{A_2}, t_{A_7}, and $t_{A_{10}}$ define positions of P-wave at 1, 2, 7, and 10 minutes, respectively, after event at point A.

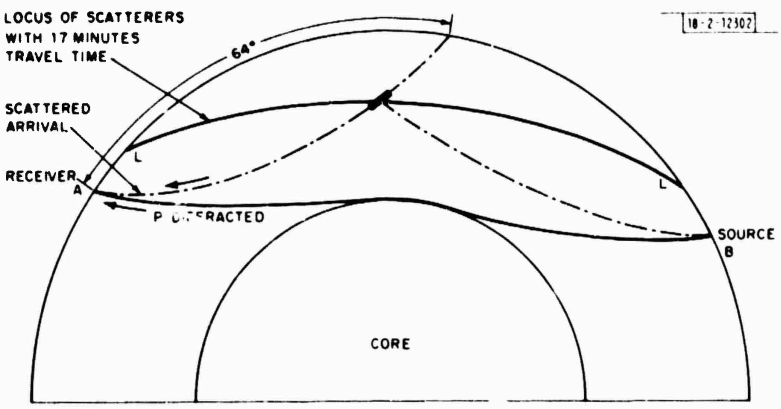

Fig. IV-8. Model for earthquake discussed in text. Line LL is "iso-time" line which represents locus of possible positions of P-P scatterers that will allow total travel time between points A and B. Intersection of this locus with ray defined at LASA array by slowness of 6.4 gives probable position of hypothesized single scatterer in mantle.

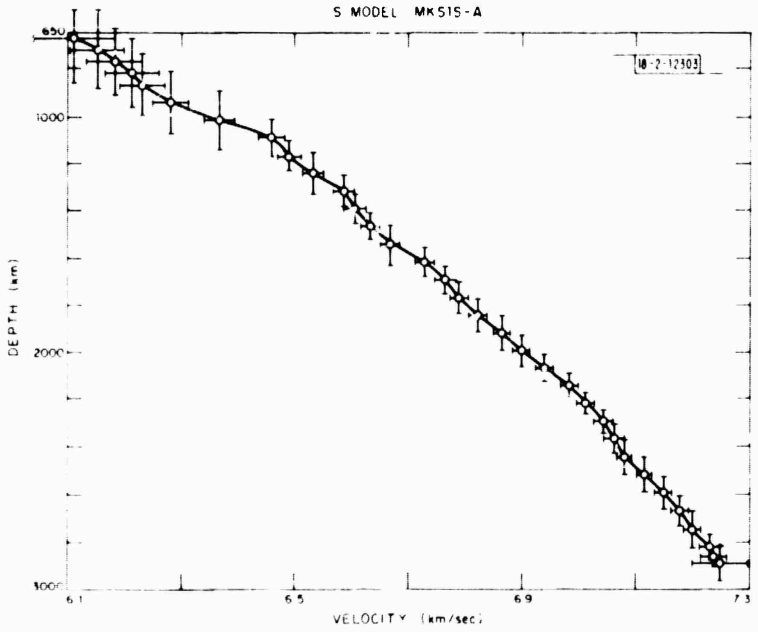

Fig. IV-9. Shear velocity model for earth's lower mantle. Horizontal and vertical error bars are explained in text.

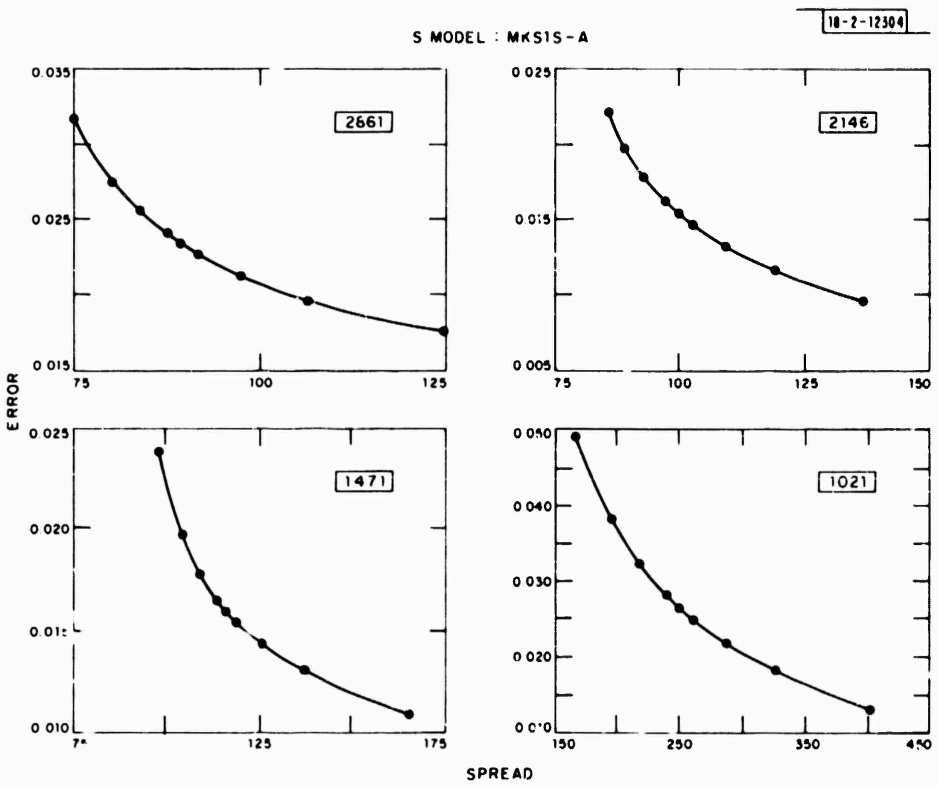

Fig. IV-10. Trade-off curves for inverted shear velocity. Depths are shown in square bars.

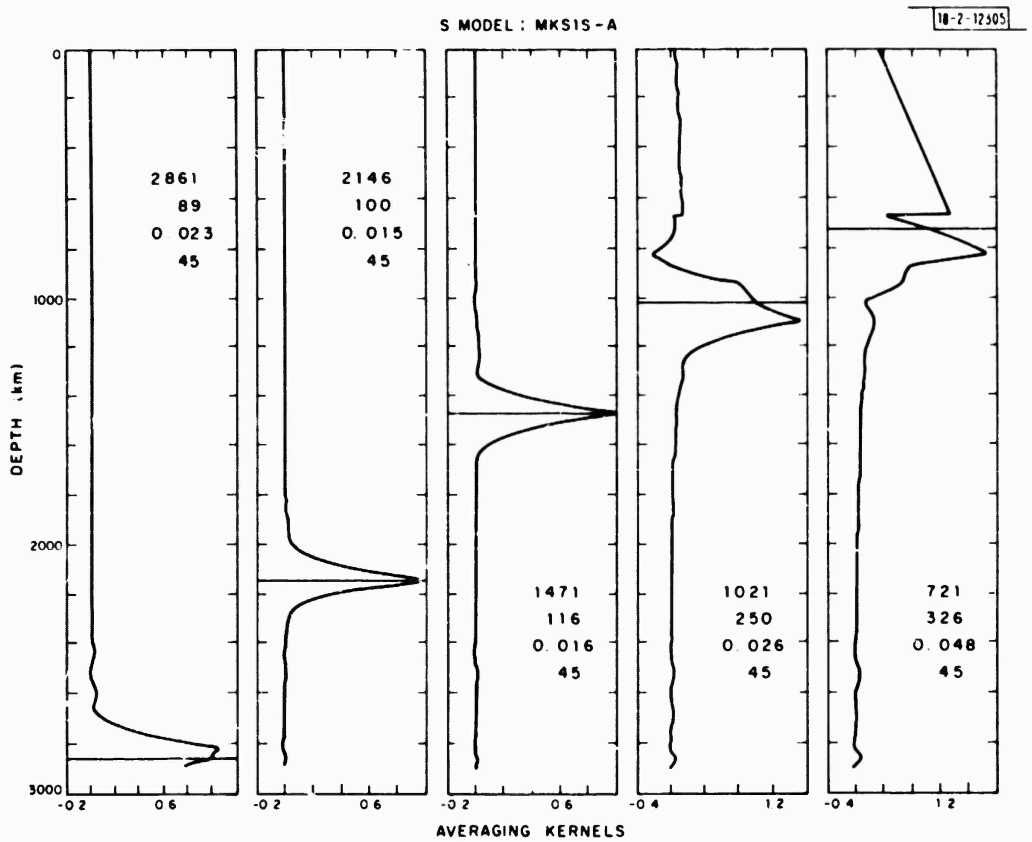

Fig. IV-11. Averaging kernels at optimum point on trade-off curves. Four numbers shown for each kernel are (from top) depth (in km), spread of kernel (in km), standard error in velocity (in km/sec), and a running parameter on the trade-off curve (in deg).

V. SOURCE MECHANISM STUDIES

A. P-WAVEFORMS FROM SHALLOW EARTHQUAKES

A significant advance might be made in discrimination seismology if we could accurately interpret the P-waveform, both long and short period, from shallow earthquake sources. Here "long and short period" refers to the response of the typical World-Wide Standard Seismographic Network (WWSSN) instruments. The interpretation of the short-period seismograms is more relevant to the discrimination problem because of their higher magnification; however, the long-period data, because of the longer wavelengths involved, are less contaminated by minor variations in structure along the path. We propose to use the long-period data as a crutch to help us identify the gross features of the source and to help us interpret salient features on the short-period records. In Fig. V-1(a), we demonstrate that this is a valid way to proceed. Trace 1 is the long-period vertical recording of a shallow Asian earthquake recorded at Berkeley, California (BKS). This trace was deconvolved with the proper instrument response to estimate ground displacement, and then reconvolved with the short-period impulse response to yield trace 2. Trace 3 is the actual short-period vertical recording at BKS of this event; most of the salient features of this trace are reproducible from the long-period record. The assertion that relevant source information exists in short-period data is supported in Fig. V-1(b) where the short-period traces from this event, recorded at two European stations (NUR and STU), are compared. These stations are at about the same azimuth from the source, but vary in epicentral distance by 15°. The first few cycles of these two waveforms are quite similar, which indicates that their basic form is due to the source, but they are dissimilar from the BKS short-period data recorded at a different azimuth. The long-period P-wave recordings of this event showed strong but regular variations as a function of azimuth.

Synthetic P-wave seismograms have been computed by many workers (notably Douglas, et al.,[1] and Helmberger[2]), and examples of these computations are shown in Fig. V-2(a-c). The upper trace in Fig. V-2(a) is the far-field P-wave radiation due to a circular strike-slip fault computed from a model developed by Savage.[3] The traces beneath this pulse represent it on short- and long-period WWSSN seismometers. In Fig. V-2(b), the middle trace represents radiation from the same fault with a surface reflection added, and the upper trace in (c) represents a multiple event of the same type without surface reflections. Beneath each of these source functions are the attendant short- and long-period seismograms. The point here is that one can qualitatively match the general features of the data shown in Fig. V-1(a-b) by the combination of proper surface reflections and, in some cases, multiple sources.

Although I don't feel confident enough in the model used to give a more specific interpretation at this time, I can make three general observations: (1) The data support earthquake models in which rupture begins at a single point rather than simultaneously along a line, (2) ambiguity will exist in most interpretations of source detail based on one or a few stations, and (3) earthquakes with discrete multiple sources are common.

J. R. Filson

B. POLARIZATION OF LONG-PERIOD BODY WAVES FROM CANNIKIN

A three-component polarization program written by Madariaga[4,5] has been modified for the data-analysis console at Lincoln Laboratory, and is being used to investigate the polarization of

waves within codas of earthquakes and explosions. The method avoids the frequency domain calculations of the polarization scheme of Shimshoni and Smith,[6] and is easier to interpret than the REMODE[7] program. Basically, this method calculates particle motion ellipses as a function of time by computing the eigenvalue λ_i and corresponding eigenfunctions $\bar{e}_i$ of the matrix

$$R = E\{\overline{XX}^T\} \tag{V-1}$$

where

$$\bar{X} = \text{col}(x, y, z) \tag{V-2}$$

is a vector of east, north, and vertical displacement components, and E is the average over a time window. The time window slides down the record, and new eigenvalues and eigenvectors are computed for each window. At a given time, the eigenvector $\bar{e}_1$ associated with the largest eigenvalue λ_1 is the direction of the most highly polarized wave, which can be P or S motion. In statistics, $\bar{e}_1$ is called the principal component and has variance λ_1. If $\lambda_1 >> \lambda_2$, then the wave is highly polarized. A single-point, adaptive filter which passes highly polarized waves is given by Madariaga[4] as

$$f = 1 - \sqrt{\lambda_2/\lambda_1} \quad . \tag{V-3}$$

The filtered output components are calculated by first projecting the principal component $\bar{e}_1$ onto each displacement component, and then scaling each component by f.

Figure V-3 shows an example of this program as applied to long-period seismograms of the explosion Carnikin, 6 November 1971, recorded at subarray 1A at NORSAR. Traces 1 to 3 are the vertical, east, and north components, respectively, of the P-wave. After rotations in the horizontal and vertical planes, the radial R, vertical Z and transverse T components are displayed in traces 4 to 6. These components are orthogonal, the radial component defined to be toward NORSAR along the incident ray direction. Traces 7 to 9 are the projections of the principal component $\bar{e}_1$ onto the rotated data using a correlation window of 20 sec. One sees that $\bar{e}_1$ is essentially parallel to the R component for the whole length of the record shown, since the projections onto Z and T components are nearly zero. Trace 10 is the filter value f as a function of time, and trace 11 is the product of f with the radial component of trace 7.

These results show that the entire coda is P-wave motion polarized in the radial direction. The program was used to determine the dip angle of the long-period first motion, assuming a back azimuth of 7.38° toward the epicenter of Cannikin, based on short-period arrivals. All subarray sites except 2B were used, yielding a dip of 73.8° ± 6.5° for 21 sites. Three sites included showed anomalously large, distorted vertical components, due apparently to a nonlinear response of the instruments to strong motion. Removing these sites gave a dip angle of 72.9 ± 3.5°. The small standard deviation suggests that these data from Cannikin are usable for long-period source studies.

C. W. Frasier

C. SURFACE WAVES FROM CENTRAL ASIAN EARTHQUAKES

Following the method of Weidner and Aki,[8] we have studied long-period Rayleigh waves from pairs of earthquakes in Central Asia. Our goal is to determine the source parameters (depth, slip, dip, strike) of these earthquakes, and then to evaluate the method by comparing our results against independent observations.

The method makes use of amplitude and phase spectra of surface waves from earthquakes which are located close together and which are known to have different fault plane solutions. In particular, the differential phase at a given observation point is defined by Weidner and Aki[8] as follows:

$$\Delta\varphi = \varphi_1 - \varphi_2 + \omega\left(T_1 - T_2 - \frac{x_1 - x_2}{c}\right)$$

where

φ_1, φ_2 = observed phase delay for events 1 and 2 in cycles/second

T_1, T_2 = difference between origin time and start of digitization for events 1 and 2 in seconds

x_1, x_2 = epicentral distances for events 1 and 2 in kilometers

ω = frequency in hertz

c = phase velocity in kilometers/second.

By taking differential phase and amplitude ratios, we hope to eliminate the propagation effects and retain the characteristics of the two sources. Using theoretical calculations based on the work of M. Saito,[9] we search parameter space for a best fit in the least-squares sense to all the observed spectral ratios.

TABLE V-1
SOURCE PARAMETERS FOR TWO CENTRAL ASIAN EVENTS

Event Number	Date	Origin Time	Latitude	Longitude	m_b
21	11 May 1967	14:50:57	39.3°N	73.7°E	5.5
22	14 Sept 1969	16:15:26	39.7°N	74.8°E	5.5

We report the progress on one earthquake pair located in the Pamir and south Tien Shan mountains. Information about this pair of events is given in Table V-1. The fault plane solutions were determined by Molnar, et al.[10] We have digitized vertical component Rayleigh waves from these events at 22 WWSSN stations, the majority of which are located on the European continent. Since the records suffered from severe interference, a time variable filter (Landisman, et al.[11]) was designed and applied to each seismogram so as to pass only fundamental mode Rayleigh waves between a 30- to 100-sec period. Spectral ratios were computed for each station in this period range, and the theoretical calculations led to the fit shown in Fig. V-4. Each graph is produced by changing a parameter, while holding the others fixed at their best value. Arrows on this graph indicate minimum in the standard deviation for differential phase. We may note here that USCGS reports a depth of 21 km for event 21, while short-period LASA records for event 22 reveal a phase, possibly pP, which places this event roughly 30 km deep.

We are encouraged by our results to date, and continue with closer analysis on more earthquake pairs.

H. J. Patton

REFERENCES

1. A. Douglas, J. Hudson and C. Blamey, "A Quantitative Evaluation of Seismic Signals at Teleseismic Distances III. Computed P and Rayleigh Wave Seismograms," Geophys. J. R. Astron. Soc. 28, 385-410 (1972).

2. D. Helmberger, "Numerical Seismograms of Long-Period Body Waves from Seventeen to Forty Degrees," Bull. Seismol. Soc. Am. 63, 633-646 (1973).

3. J. Savage, "Radiation from a Realistic Model of Faulting," Bull. Seismol. Soc. Am. 56, 557-592 (1966).

4. R. Madariaga, "Procesamiento Automatico de Sismogramas Mediante el Analysis Espectral y Filtros de Polarization," Thesis, University of Chile, Faculty of Physical Sciences and Mathematics, Department of Geophysics and Geodesy (1967).

5. E. S. Husebye, A. Christoffersson and C. Frasier, "Orthogonal Representation of Array-Recorded Short Period P Waves," NATO Advanced Study Institute – "Exploitation of Seismograph Networks," Proceedings, 10 May 1974.

6. M. Shimshoni and S. Smith, "Seismic Signal Enhancement with Three Component Detectors," Geophys. 29, 664-671 (1964).

7. C. H. Mims and R. . Sax, "Rectilinear Motion Detection (REMODE)," Seismic Data Laboratory Report No. 118, Earth Sciences Division, Teledyne, Inc. (1965).

8. D. J. Weidner and K. Aki, "Focal Depth and Mechanism of Mid-Ocean Ridge Earthquakes," J. Geophys. Res. 78, 1818 (1973).

9. M. Saito, "Excitation of Free Oscillations and Surface Waves by a Point Source in a Vertically Heterogeneous Earth," J. Geophys. Res. 72, 3689 (1967).

10. P. Molnar, T. J. Fitch and F. T. Wu, "Fault Plane Solutions of Shallow Earthquakes and Contemporary Tectonics in Asia," Earth and Planet. Sci. Ltrs. 19, 101 (1973).

11. M. Landisman, A. Dziewonski and U. Sato, "Recent Improvement in the Analysis of Surface Wave Observations," Geophys. J. R. Astron. Soc. 17, 369 (1969).

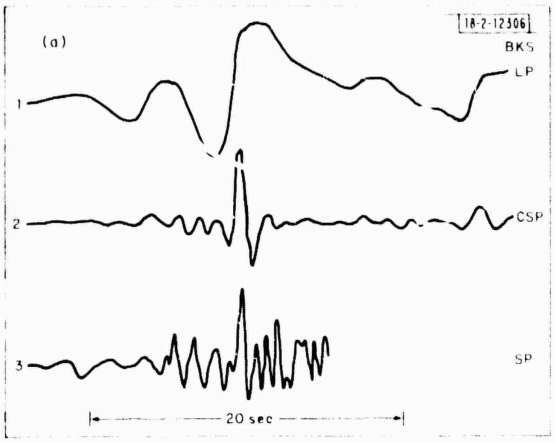

Fig. V-1(a-b). Short- and long-period seismograms from shallow Asian earthquake.

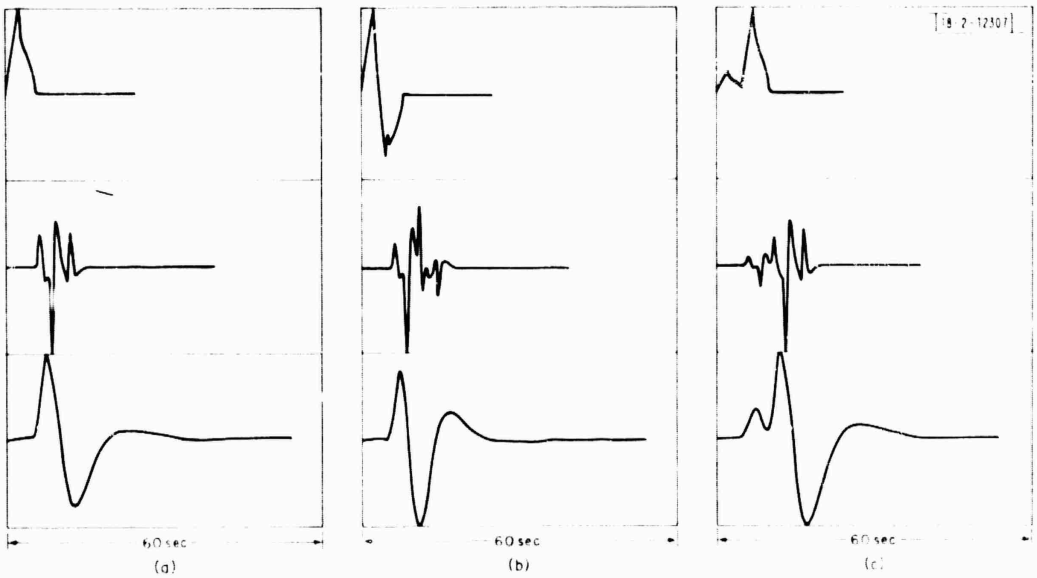

Fig. V-2(a-c). Far-field source pulses and synthetic seismograms based on theoretical fault model.

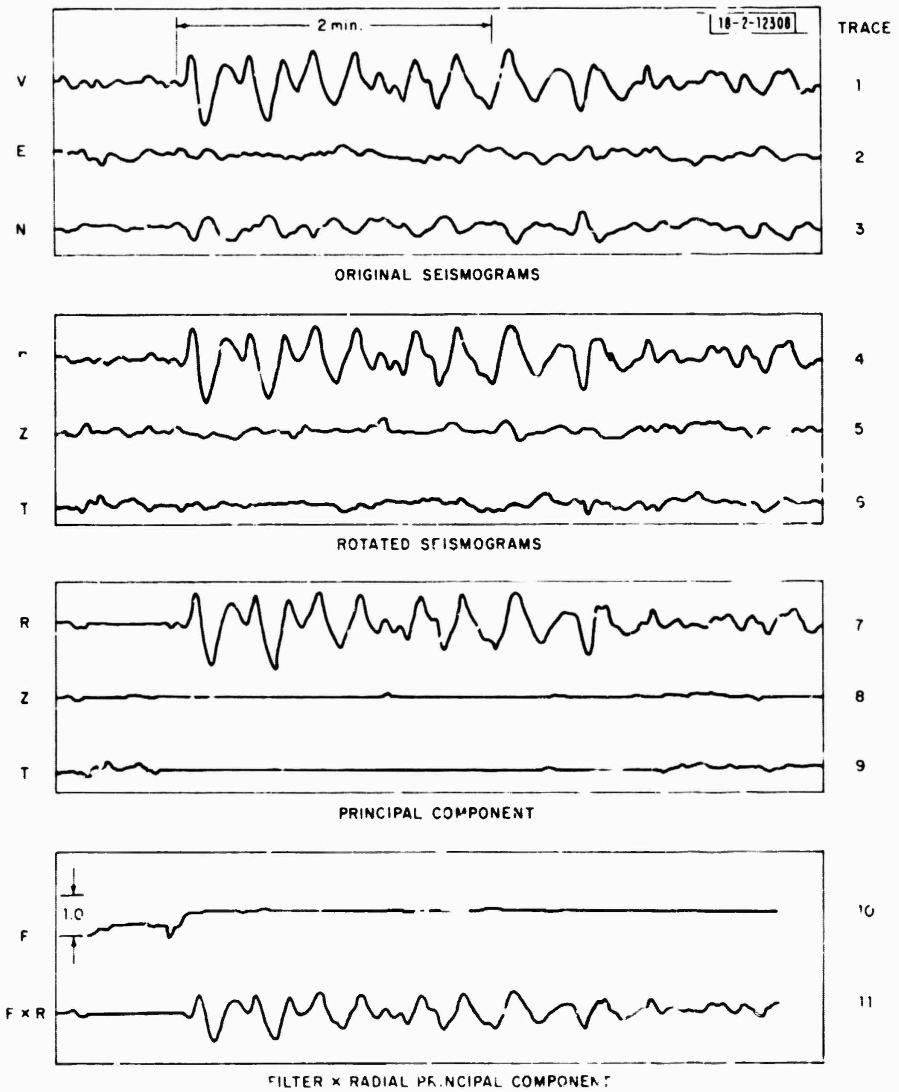

Fig. V-3. Example of polarization method. Traces 1 to 3 are vertical, east, and north components of long-period P-wave from explosion Carnikin, 6 November 1971, recorded at subarray 1A of NORSAR. Rotated components are traces 4 to 6, R being radial component toward receiver along ray path; T is transverse horizontal component, and Z is upward in vertical plane, orthogonal to T and R. Traces 7 to 9 are projections of principal component onto R, Z, and T axes. Trace 10 is polarization filter, and trace 11 is product of traces 7 and 10.

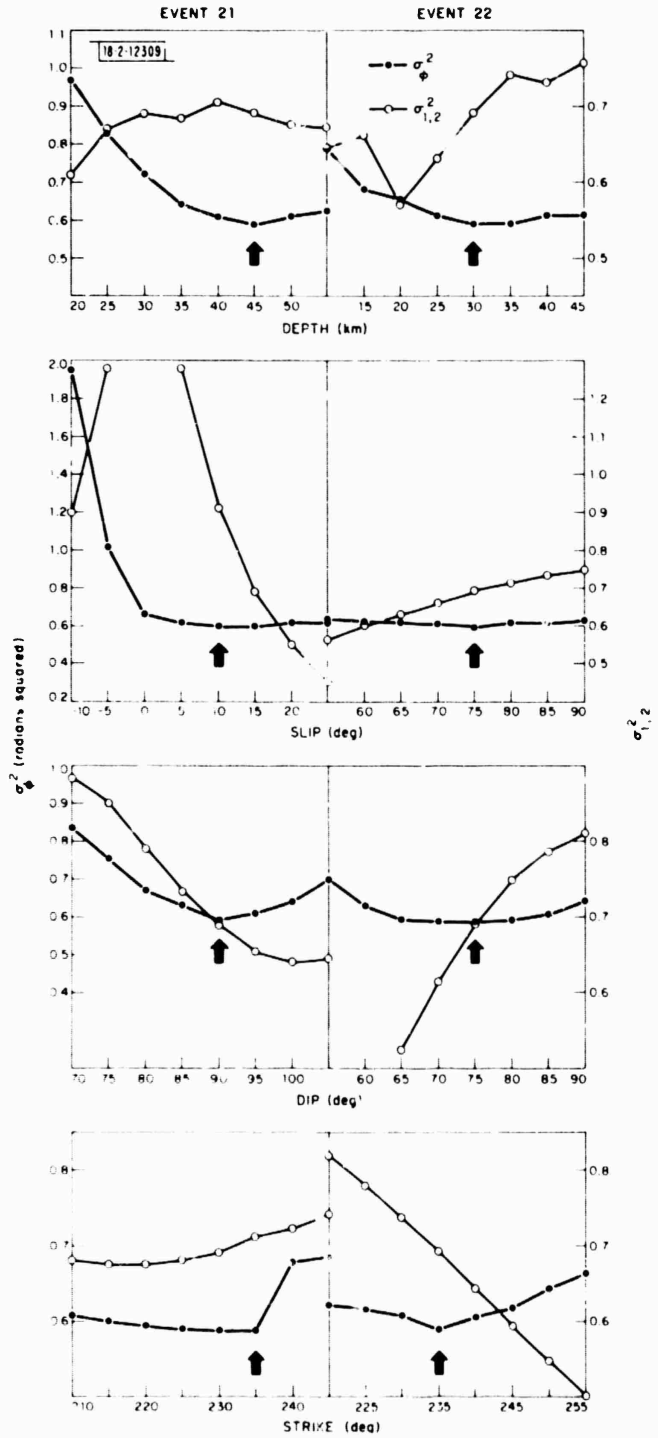

Fig. V-4. Results of fit to observed spectral ratios. $\sigma_{1,2}^2$ is weighted sum of squares over frequency and station of observed log amplitude ratio minus theoretical log amplitude ratio. σ_ϕ^2 is similar weighted sum of squares of observed differential phases minus theoretical differential phase. For details, these quantities are given in Weidner and Aki.[8]

VI. GLOBAL SEISMIC ACTIVITY

A. CHARACTERISTICS OF SHORT-TERM VARIATIONS IN SEISMIC ACTIVITY

It is well known that seismic activity varies from time to time, although the characteristics of this variation are not well understood. The presence of this variation impacts on the discrimination problem in several ways. In order to evaluate the effectiveness of a seismic network, it is common to count the events detected during a limited period (for example, the International Seismic Month[1]). Estimates of the level of background seismic activity and the rate of occurrence of anomalous events are frequently obtained in the same way. It is usually not clear whether the sample discussed is a good representation of the seismic activity to be expected at some future time. It is possible, for example, that a network processing scheme designed to handle the long-term average rate of seismicity in real time may become swamped with events during an activity maximum.

Evidence[2] has been given that the PDE earthquake listing is approximately complete for magnitudes (m_b) greater than 5.1. We have therefore used this list as a basic data set. Figure VI-1 shows the number of events listed during successive 40-day intervals for the period 1966 to 1974, for $m_b \geq 5.2$, $m_b \geq 5.5$, and $m_b \geq 5.8$. The period of 40 days was chosen as being short enough to show rapid fluctuations in activity, but long enough to include sufficient events for an adequate data sample.

Figure VI-1 has many features of interest. First, the fluctuations in event numbers are considerable. For example, events with $m_b \geq 5.5$ range from a minimum of 9 to a maximum of 66 per 40-day period. Second, the changes are frequently very abrupt. Particularly rapid changes are shown during April 1968, June 1971, July 1972, and June 1973. Potential reasons for these changes are under investigation.

Perhaps the most important aspect of Fig. VI-1 is that the fluctuations in activity appear approximately independent of magnitude. To illustrate this, Fig. VI-2 shows the ratio of the number of events with $m_b \geq 5.2$ to the number with $m_b \geq 5.5$, and also the ratio for $m_b \geq 5.5$ to $m_b \geq 5.8$. With the exception of a few unusually large values, these ratios show remarkable stability. This implies that the frequency-magnitude curve is fluctuating rapidly parallel to the frequency axis, with very little change in shape. (There is some evidence for a long-term change in shape, which is small but persistent.) We prefer to use the term "change in shape" rather than change in b-value since we have shown earlier[2] that the global frequency-magnitude (m_b) curve is not linear.

We conclude from this study that seismic activity appears to have real short-term variations in level that are considerable in size. Further investigations of this phenomenon are continuing.

M. A. Chinnery

B. SPECTRAL ANALYSIS OF EARTHQUAKE OCCURRENCE RATES

In the previous SATS,[2] the level of seismic activity was shown to be a time-dependent function, independent of the magnitude range over which it is determined. Evidence showing that periodicities exist in this function would be of fundamental importance to several seismic discrimination problems. For example, the ability to hide an explosion in an earthquake is highly dependent on the rate at which suitably large enough earthquakes occur. Knowledge of a time interval during which large earthquakes are highly likely to occur would make such a scheme

Preceding page blank

more feasible. Evidence for periodicities in the rate function would also indicate what controls the initiation of rupture. If the rate function is random, one can conjecture that the physical characteristics in the focal region control whether or not an earthquake will occur. On the other hand, if it is periodic then the occurrence of earthquakes may be more directly in response to regional stress fields generated perhaps by flow in the asthenosphere. Of course, the real situation is at best a mixture, the proportions of the mix being determined by the relative power contained in the periodic part of the spectrum of the rate function.

The problem of determining whether or not a function is random or periodic can be approached by comparing an estimate of the power at a given period with the power that might by chance appear at that period if an equal length of random data was analyzed. The spectrum from a finite segment of random data will be peaked and not necessarily flat. The fact that it is random just implies that the average of a large ensemble of spectra of the sequence will tend to be white. Consequently, when dealing with finite lengths of data, spectral peaks must be assigned a degree of significance compared with a specific random process. Many authors have pointed out that spectral peaks for earthquake occurrence rate data are highly significant compared with those expected from random data, with a Poisson distribution function assuming independent events. They usually conclude, though, that if the events were somewhat mutually dependent, the periodicities would not be significantly nonrandom. The difficulty in determining that random process to compare data can be circumvented somewhat if several estimates of the spectrum of the data can be made from partially or totally independent segments. The nonrandom spectral peaks should be present in each estimate. Peaks from random data should not coincide, and simultaneously have the same shape so that the average spectrum will tend to be white. This behavior is independent of the probability distribution function of the random process.

The practical problem is that if the length of the available rate data is short, then a reliable spectral estimate is difficult, if not impossible, to make. A recent innovation, due to John Burg of Stanford University, for computing the autocorrelation function for short sequences makes it possible to overcome this problem. The following figures present the results of using Maximum Entropy Spectral Analysis, using the Burg technique for computing the prediction error wavelet, to determine the nonrandom periodic behavior of Global Earthquake Occurrence Rate data.

Figure VI-3 shows the earthquake occurrence rate computed using all earthquakes in the PDE with $m_b \geq 5.5$ from 1964 to the present. $m_b \geq 5.5$ was chosen because the catalog is essentially complete above this threshold. Taking a limited range is justified by evidence that the time dependence of the frequency of earthquakes is independent of magnitude range. We chose to start at 1966 since a large single swarm in the Rat Islands dominates the data previous to this date. The rate was determined using a time interval of 40 days. The total number of points amounts to 72 and covers about 8 years. Forty-day averaging also acts as an anti-aliasing filter for any high-frequency power that might exist at the tidal periods. The idea was to divide these 72 points into several segments, make a spectral estimate of each, and look for the coincidence of spectral peaks. If the rate function is random, the spectral average will tend to be white. Figure VI-4 shows a random sequence of numbers with a Poisson probability distribution function that was treated exactly the same as the rate data to illustrate the previously mentioned behavior.

Figure VI-5 illustrates why one needs to make several estimates of the spectra and why simple FFT estimates are not sufficient to do this. The upper curve is the FFT spectrum based

on 64 points of the rate data. Directly below it is the Burg Maximum Entropy (BME) spectrum for the same data. At the bottom is the BME spectrum for 64 points of the random data. By comparing the bottom two spectra, it is clear that one cannot say whether the apparent periodicities in the rate data are random or real. The FFT shows essentially the same peaks as the Burg spectrum, but with much less resolution. If the data were divided into two 32-point segments and the spectra were computed, the FFT spectra would have little resolution and further, and probably worse, the end conditions implicit in the FFT would make the resulting spectra unreliable. There is, for example, only one point in the FFT spectrum between the peaks near 0.1 and 0.13 cycles per month. In the BME spectra, about 400 points are plotted between the two peaks.

Figure VI-6(a-c) shows how the spectra, computed from 3 segments of the random data, do not coincide. Each segment is 40 points long so that the middle segment overlaps half of the first and last segments. A filter length of 25 was used. The spectra are clearly uncorrelated. Using exactly the same procedure for dividing the rate data and using the same filter length, we computed the spectra shown in Fig. VI-7(a-c). There is a triple coincidence of peaks for periodicities at 9.3 and 7.5 months. The other peaks have no nonrandom significance. The slight shift in the bottom to 7.6 months is not significant. In the BME method, when noise is present and relatively long filters are used, such shifts are common, but not serious in this study.

Since resolution is so sharp and because of noise and filter length effects, absolute amplitudes using the BME method are often unreliable. However, the integrated power under each peak proves to be quite accurate. Figure VI-8(a-b) compares the accumulated power of the spectra for the rate data and the random data, and shows that about 30 percent of the total power is contained in the bands 9.3 ± 0.3, and 7.5 ± 0.3 months. The average of the accumulated power for the random data tends to a straight line, indicating whiteness.

In summary, to a high degree of certainty, periodicities at 7.5 and 9.3 months exist in the earthquake rate from 1966 to the present, and these periods contain approximately 30 percent of the total power in the data. The physical significance of this is yet to be determined, but there are no externally produced strains in the crust with these periods and it seems likely that we are observing a characteristic of a global internally induced strain.

T. E. Landers
M. A. Chinnery

REFERENCES

1. R. T. Lacoss, R. E. Needham and B. R. Julian, "International Seismic Month Event List," Technical Note 1974-14, Lincoln Laboratory, M.I.T. (27 February 1974), DDC AD-776021/8.
2. Seismic Discrimination SATS, Lincoln Laboratory, M.I.T. (30 June 1974), DDC AD-785377/3.

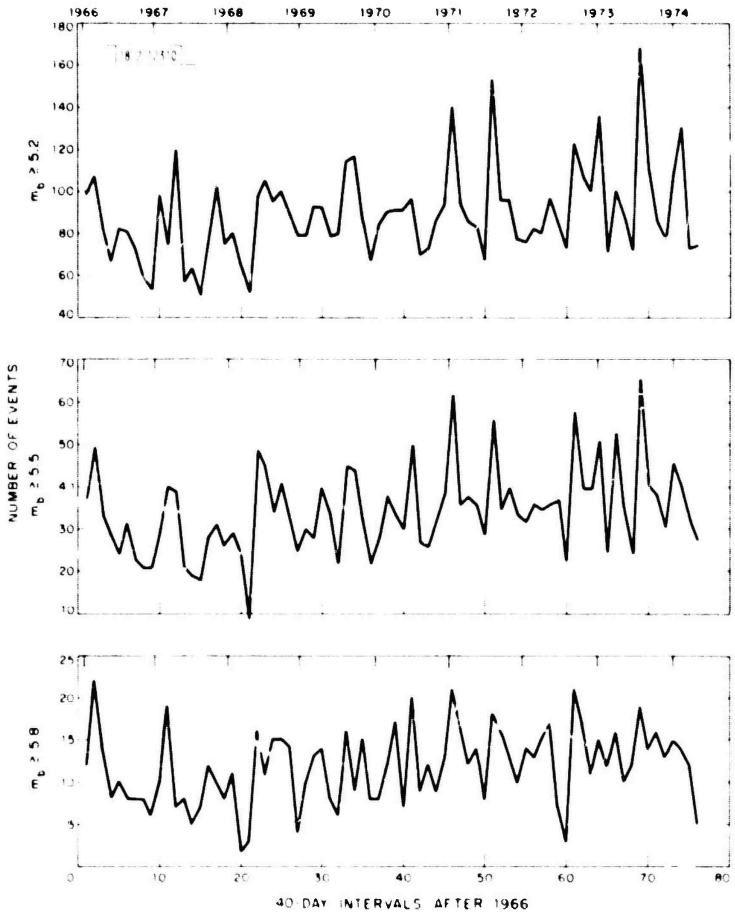

Fig. VI-1. Earthquake counts for successive 40-day intervals from PDE earthquake listing for period January 1966 to April 1974.

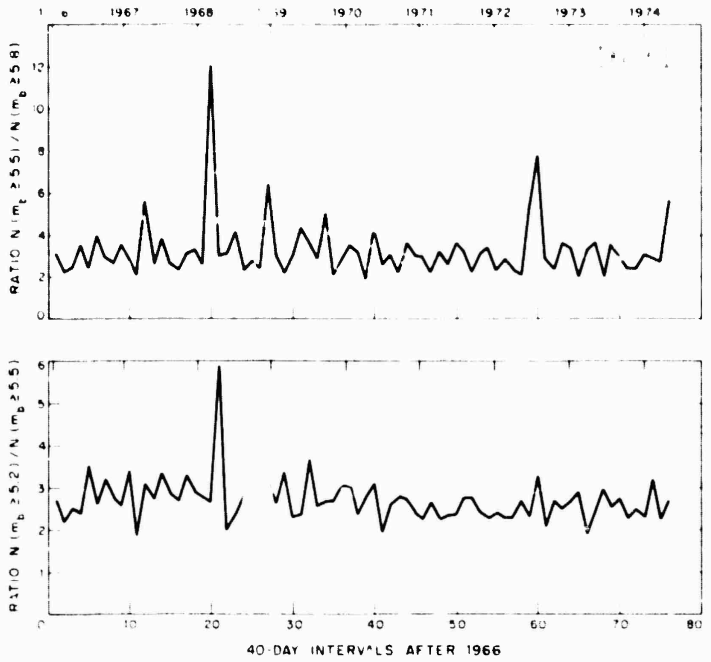

Fig. VI-2. Ratios of earthquake counts shown in Fig. VI-1.

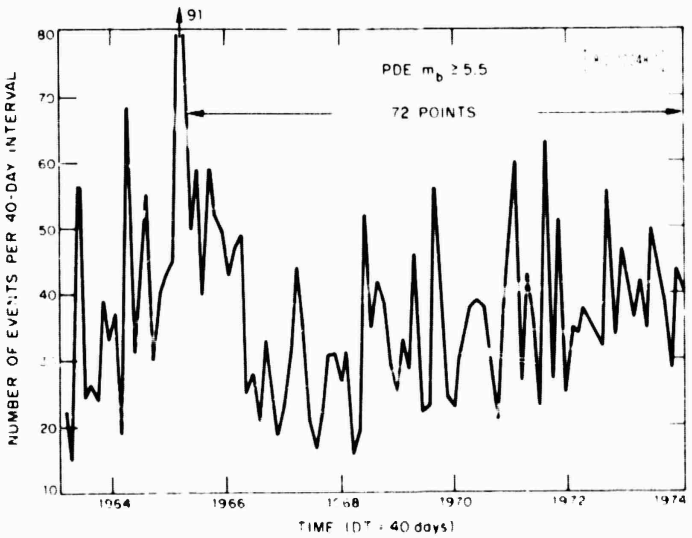

Fig. VI-3. Earthquake occurrence rate per 40-day interval, 1964 to present.

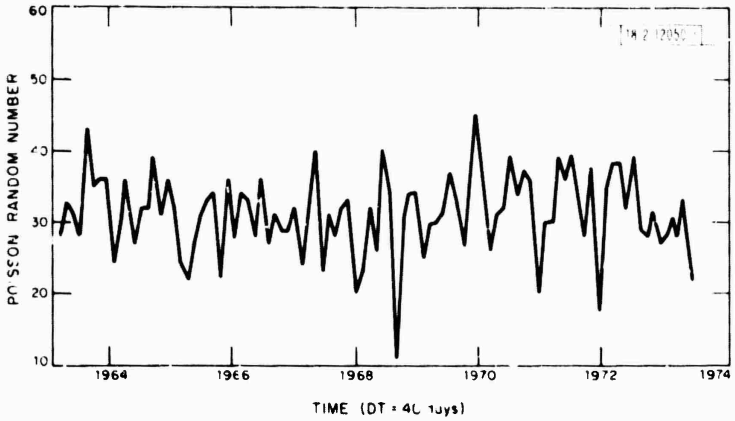

Fig. VI-4. Random numbers with mean of 30 and Poisson probability distribution at 40-day intervals, 1964 to present.

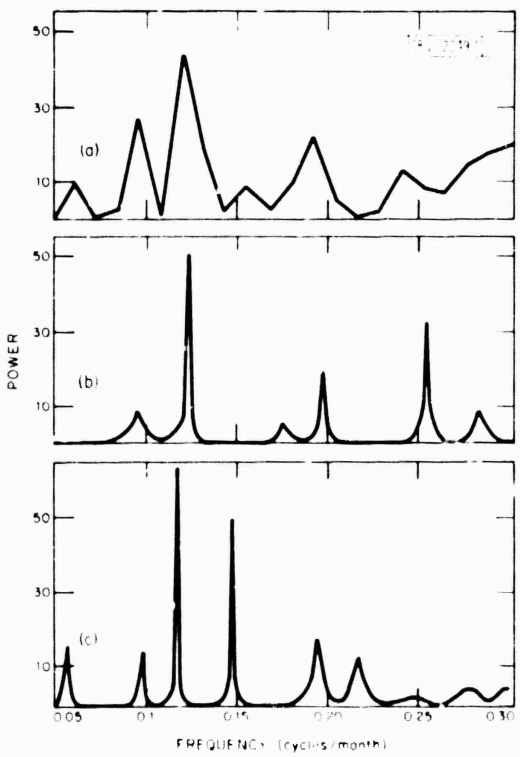

Fig. VI-5. (a) FFT power spectrum of 64 points of earthquake occurrence rate; (b) BME power spectrum of same data; and (c) BME power spectrum of 64 points of Poisson random data.

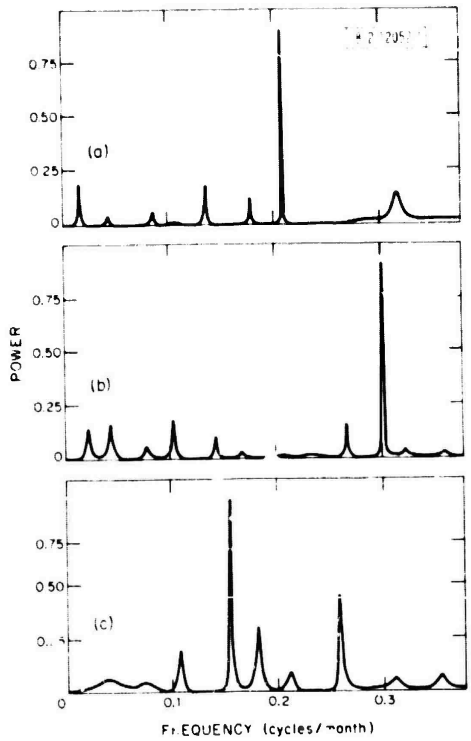

Fig. VI-6. BME power spectra for three 40-point segments of random data. (a) First half, (b) middle, and (c) last half of data.

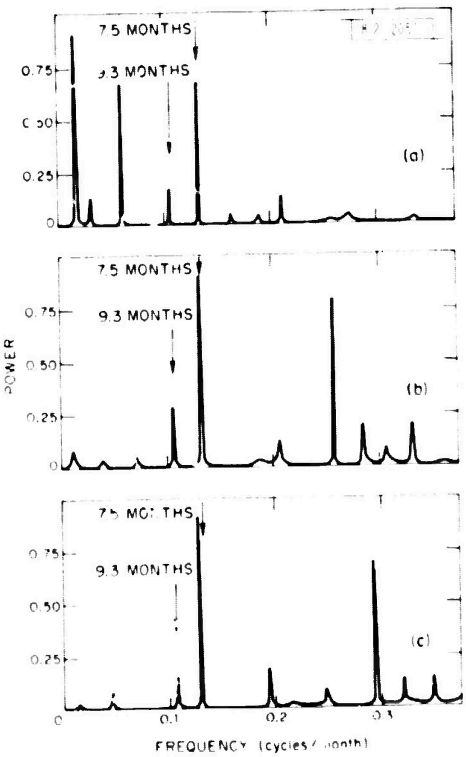

Fig. VI-7. BME power spectra for three 40-point segments of earthquake occurrence rate. Peaks at 9.3 and 7.5 months coincide, indicating continuing power at those periods over complete time span. (a) First half, (b) middle, and (c) last half of data.

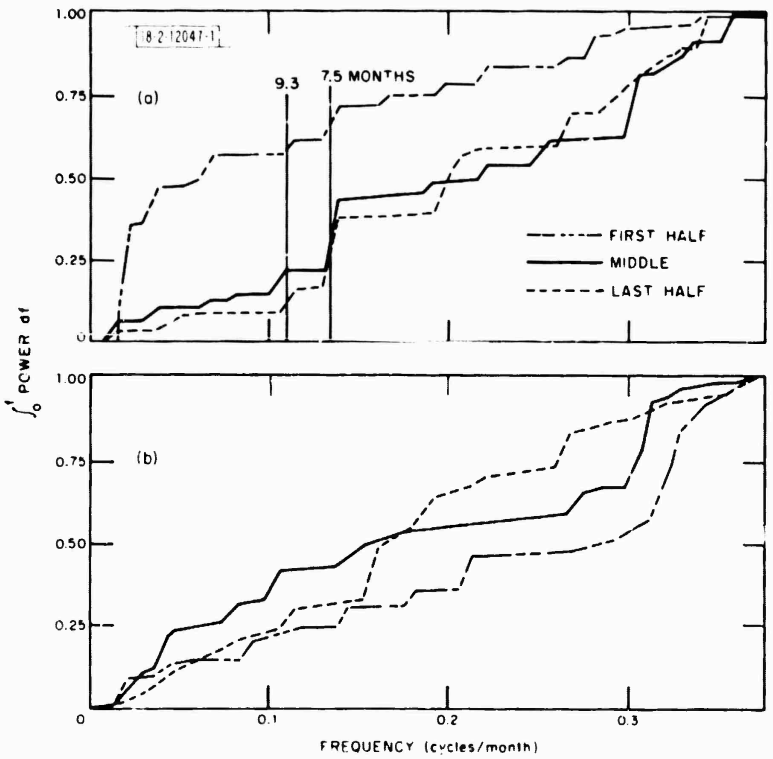

Fig. VI-8. Integrated power from 0 to f of BME spectra for occurrence rate and random data. Approximately 30 percent of total power in occurrence rate lies in bands 9.3 ± 0.3, and 7.5 ± 0.3 months. (a) Earthquake catalog and (b) Poisson random data.